X-ray constrained Spin-Coupled Technique: Theoretical Details and Further Assessment of the Method

Authors

Alessandro Genoni[a]*, Giovanni Macetti[a], Davide Franchini[b], Stefano Pieraccini[bcd] and Maurizio Sironi[bcd]

[a]Université de Lorraine & CNRS, Laboratoire de Physique et Chimie Théoriques, 1 Boulevard Arago, Metz, F-57078, France

[b]Dipartimento di Chimica, Università degli Studi di Milano, Via Golgi 19, Milano, I-20133, Italy

[c]Istituto di Scienze e Tecnologie Molecolari (ISTM), CNR, Via Golgi 19, Milano, I-20133, Italy

[d]Consorzio Interuniversitario Nazionale per la Scienza e Tecnologia dei Materiali (INSTM), UdR Milano, Via Golgi 19, Milano, I-20133, Italy

Correspondence email: Alessandro.Genoni@univ-lorraine.fr

Funding information A.G. and G.M. acknowledge the French Research Agency (ANR) for financial support of the Young Researcher Project QuMacroRef (grant No. ANR-17-CE29-0005-01 to Alessandro Genoni).

Synopsis In this paper, we present in details a new method that extends the Jayatilaka X-ray constrained wave function approach in the framework of the Spin-Coupled technique of the Valance Bond theory. The proposed strategy enables the extraction of traditional chemical information (e.g., weights of resonance structures) from experimental X-ray diffraction data without imposing constraints *a priori* or performing further analyses a *posteriori.* Compared to the preliminary version of the method, X-ray constrained Hartree-Fock molecular orbitals are used in the calculations and a more balanced description of the electronic structure and better electron densities are obtained.

Abstract Nowadays, one of the well-established methods of modern Quantum Crystallography is undoubtedly the X-ray constrained wave function (XCW) approach, a technique that enables the determination of wave functions that not only minimize the energy of the system under examination, but that also reproduce experimental X-ray diffraction data within the limit of the experimental errors. Initially proposed in the framework of the Hartree-Fock method, the strategy has been gradually extended to other techniques of Quantum Chemistry, but always remaining limited to a single-determinant *ansatz* for the wave function to extract. This limitation has been recently overcome through the development of the novel X-ray constrained Spin-Coupled (XCSC) approach (Genoni, Franchini *et al.*, 2018) that merges the XCW philosophy with the traditional Spin-Coupled strategy of Valence Bond theory. The main advantage of this new technique is the possibility of extracting traditional chemical descriptors (e.g., resonance structure weights) compatible with the experimental

diffraction measurements, without the need of introducing information *a priori* or performing analyses *a posteriori*. In this paper, we provide a detailed theoretical derivation of the fundamental equations at the basis of the XCSC method and we also introduce a further advancement of its original version, mainly consisting in the use of molecular orbitals resulting from XCW calculations at Hartree-Fock level to describe the inactive electrons in the X-ray constrained Spin-Coupled computations. Furthermore, we present and discuss extensive test calculations that we have performed by exploiting high-resolution X-ray diffraction data for salicylic acid and by adopting different basis-sets. The computational tests have shown that the new technique does not suffer of particular convergence problems. Moreover, all the XCSC calculations provided resonance structure weights, spin-coupled orbitals and global electron densities slightly different form those resulting from the corresponding unconstrained computations. These discrepancies can be ascribed to the capability of the novel strategy in capturing the information intrinsically contained in the experimental data used as external constraints.

Keywords: X-ray constrained wave function; Quantum Crystallography; Valence Bond theory; Spin-Coupled method.

1. Introduction

As is well known, in theoretical chemistry there exist two main approaches to investigate molecular electronic structure: the Valence Bond (VB) (Heitler & London, 1927; London, 1928; Pauling, 1939) and the Molecular Orbital (MO) (Hückel, 1930; Hückel, 1931; Roothaan, 1951; Dewar, 1952) theories. The former has been strictly related to the traditional chemical perception since its origin and significantly contributed to the definition of concepts (e.g., Lewis structures, resonance structure, hybridization, local bonds, electronegativity, *etc.*) that, even today, are of customary use among chemists and constitute the basis of the traditional chemical reasoning to interpret bonding and reactivity. On the contrary, the latter provides pictures of the electronic structure that are generally delocalized over the whole molecules under exam and that are consequently far from the traditional chemical notions. Despite this fact, the MO-based methods have become more and more predominant in electronic structure investigations, mainly due to their high predictive power, their intrinsic lower computational cost (at least for the basic strategies) and the ease with which they could be implemented into working computer codes (Shurki, 2006; Hiberty, 2007). Nevertheless, owing to the unquestionable higher chemical interpretability associated with the VB theory, different Valence Bond approaches have been continuously proposed over the years (Shurki, 2006; Hiberty & Shaik, 2007; Goddard, 1967; Ladner & Goddard, 1969; Goddard *et al.*, 1973; Gerratt & Lipscomb, 1968; Gerratt, 1971; Cooper *et al.*, 1986; Cooper *et al.*, 1991; Karadakov *et al.*, 1992; Cooper *et al.*, 1993; Raimondi *et al.*, 1996; Thorsteinsson *et al.*, 1996; Hirao *et al.*, 1996; Voter & Goddard, 1981;

Hollauer & Nascimento, 1993; McDouall, 1992; van Lenthe & Balint-Kurti, 1983; Hiberty *et al.*, 1994; Song *et al.*, 2003), each of them with its own features and with its main field of application. In this paper, we will particularly consider the Spin-Coupled (SC) method (Gerratt & Lipscomb, 1968; Gerratt, 1971; Cooper *et al.*, 1986; Cooper *et al.*, 1991; Karadakov *et al.*, 1992; Cooper *et al.*, 1993; Raimondi *et al.*, 1996), a technique that uses a very general single-configuration wave function by including all the possible spin-coupling modes and without imposing any constraints (e.g., orthogonality constraints) on the orbitals expansions. Despite its intrinsically correlated nature, the approach keeps a high-degree of chemical interpretability. For example, the coefficients associated with the spin-coupling modes considered in the wave function are generally interpreted as a measure of the weights corresponding to the resonance structures of the investigated system, while the spatial extensions of the SC orbitals are generally exploited to get insights into the electron distributions around atoms and, consequently, into the atomic hybridizations.

Therefore, due to the wealth of information that one can generally extract from SC wave functions, we have recently combined the Spin-Coupled method of the Valence Bond theory with the X-ray constrained wave function (XCW) philosophy (Jayatilaka, 1998; Jayatilaka & Grimwood, 2001; Grimwood & Jayatilaka, 2001; Bytheway, Grimwood & Jayatilaka, 2002; Bytheway, Grimwood, Figgis *et al.*, 2002; Grimwood *et al.*, 2003; Hudák *et al.*, 2010; Jayatilaka, 2012; Bučinský *et al.*, 2016), thus giving rise to the novel X-ray constrained Spin-Coupled (XCSC) technique (Genoni, Franchini *et al.*, 2018), with the final goal of proposing another useful method to extract chemical information directly from experimental X-ray diffraction data.

In fact, along with strategies as the multipole models (Stewart, 1976; Hansen & Coppens, 1978) and the maximum entropy methods (MEM) (Sakata & Sato, 1990; Roversi *et al.*, 1998; Van Smaalen & Netzel, 2009), which are density-based approaches, the XCW technique introduced by Jayatilaka in 1998 (Jayatilaka, 1998) is currently one of the most important methods in the rising field of Quantum Crystallography (Genoni, Bučinský *et al.*, 2018; Novara *et al.*, 2018; Grabowsky *et al.*, 2017; Massa & Matta, 2017; Tsirelson, 2017) and probably the most popular tool to extract wave functions and/or density matrices from experimental X-ray diffraction and/or scattering measurements. Its roots obviously date back to the pioneering methods proposed by Clinton, Massa and their coworkers to obtain *N*-representable one-electron density matrices from X-ray diffraction data (Clinton & Massa, 1972; Clinton *et al.*, 1973; Frishberg & Massa, 1981; Goldberg & Massa, 1983; Massa *et al.*, 1985). Inspired by these works, different researchers have devised alternative techniques to determine "experimental" wave functions/density matrices (Aleksandrov *et al.*, 1989; Howard *et al.*, 1994; Snyder & Stevens, 1999; Tanaka, 1988; Tanaka, 2018; Hibbs *et al.*, 2005; Waller *et al.*, 2006; Schmider *et al.*, 1990; Schmider *et al.*, 1992; Weyrich, 2006; Gillet *et al.*, 2001; Gillet & Becker, 2004; Gillet, 2007; Guedidda *et al.*; 2018). Among them, it is worth citing Tanaka's X-ray Atomic Orbital (XAO) (Tanaka, 1988) and X-ray Molecular Orbital (XMO) (Tanaka, 2018) methods, the

Molecular Orbital Occupation Number (MOON) approach (Hibbs *et al.*, 2005; Waller *et al.*, 2006) and, above all, the strategies introduced by Weyrich & Smith (Schmider *et al.*, 1990; Schmider *et al.*, 1992; Weyrich, 2006) and by Gillet, Becker and coworkers (Gillet *et al.*, 2001; Gillet & Becker, 2004; Gillet, 2007; Guedidda *et al.*; 2018) to reconstruct both the diagonal and the off-diagonal parts of the one-electron density matrices through joint refinements of X-ray diffraction data, magnetic structure factors and inelastic Compton scattering measurements. However, the above-mentioned Jayatilaka's XCW approach (Jayatilaka, 1998; Jayatilaka & Grimwood, 2001; Grimwood & Jayatilaka, 2001) represents the major breakthrough in this research field. In fact, bearing in mind Gilbert's corollary to Coleman's theorem (Gilbert, 1975), according to which there is in principle an infinite number of wave functions compatible with a given electron density, Jayatilaka proposed a method that can be considered as a practical implementation of Henderson & Zimmermann's idea (Henderson & Zimmermann, 1976) and that consists in finding wave functions that not only fit a set of diffraction/scattering data within the limit of the experimental uncertainties (as in all the other methods mentioned above), but that also minimize the energy of the systems under exam.

Originally devised in the framework of the Restricted Hartree-Fock (RHF) formalism (Jayatilaka, 1998; Jayatilaka & Grimwood, 2001; Grimwood & Jayatilaka, 2001; Bytheway, Grimwood & Jayatilaka, 2002; Bytheway, Grimwood, Figgis *et al.*, 2002; Grimwood *et al.*, 2003; Jayatilaka, 2012), the XCW method has been progressively improved by combining it to other strategies of quantum chemistry, such as the unrestricted Hartree-Fock technique (Hudák *et al.*, 2010), relativistic approaches (particularly, the second-order Douglas-Kroll-Hess (Hudák *et al.*, 2010) and the Infinite-Order Two-Component (Bučinský *et al.*, 2016) methods) and Density Functional Theory (DFT) (Jayatilaka, 2012). Therefore, the proposed XCW strategies have been mainly developed in combination with Molecular Orbital approaches, thus providing completely delocalized pictures of molecular electronic structures. To recover the traditional chemical interpretability from the obtained "experimental" wave functions, suitable *a posteriori* techniques have been exploited, as done for example by Jayatilaka, Grabowsky and coworkers (Jayatilaka & Grimwood, 2004; Grabowsky *et al.*, 2010; Grabowsky *et al.*, 2011; Grabowsky *et al.*, 2012), who have successfully applied topological strategies (e.g., Quantum Theory of Atoms in Molecules (QTAIM) (Bader, 1990), the Electron Localization Function (ELF) (Becke & Edgecombe, 1990), the Electron Localizability Indicator (ELI) (Kohout, 2004) and the Localized Orbital Locator (LOL) (Schmider & Becke, 2000)) to get back to the traditional bonding patterns for the investigated systems. For the sake of completeness, another possibility suggested by the Grabowsky group is the application of the Natural Bond Orbitals (NBO) method (Weinhold & Landis, 2001) and of the Natural Resonance Theory (NRT) (Glendening & Weinhold, 1998) to determine the weights of the resonance structures for the molecules under exam (Fugel, Klemiss *et al.*, 2018; Fugel, Beckmann *et al.*, 2018).

Before the recent introduction of the XCSC method (Genoni, Franchini *et al.*, 2018), which will be described in detail in this paper, the only techniques that allowed to directly obtain X-ray constrained wave functions already close to the traditional chemical perception without the application of subsequent bonding-analyses were the XC-ELMO (Genoni, 2013a; Genoni, 2013b; Dos Santos *et al*., 2014; Genoni & Meyer, 2016) and XC-ELMO-VB (Genoni, 2017; Casati *et al*., 2017) approaches, even if both of them are characterized by the introduction of preliminary chemical constraints. In fact, the XC-ELMO really provides X-ray constrained molecular orbitals strictly localized on elementary molecular fragments corresponding to atoms, bonds and functional groups, namely the so-called Extremely Localized Molecular Orbitals (ELMOs) (Stoll *et al.*, 1980; Fornili *et al.*, 2003; Genoni & Sironi, 2004; Genoni, Fornili & Sironi, 2005; Genoni *et al.*, 2005; Sironi *et al*, 2007; Sironi *et al*, 2009; Meyer *et al.*, 2016a; Meyer *et al.*, 2016b; Meyer & Genoni, 2018). Nevertheless, it is the user that preliminarily decides the fragmentation of the molecules into subunits according to the chemical intuition or the specific computational needs, thus partially biasing the results of the calculations. In a quite analogous way, in the XC-ELMO-VB method the global wave function is written as a linear combination of pre-computed ELMO wave functions corresponding to the different resonance structures that one wants to take into account, but, during the computations, only the weights of these resonance structures are determined, while the ELMO wave functions remain unchanged.

This scenario has thus prompted us to develop a novel XCW technique able to extract chemically meaningful information from X-ray diffraction data without applying *a posteriori* techniques for the analysis of the obtained "experimental" wave functions or without imposing chemical constraints *a priori*. As mentioned above, this has been accomplished through the development of the new X-ray constrained Spin-Coupled method (Genoni, Franchini *et al.*, 2018), which is the extension of the X-ray constrained wave function approach to the Spin-Coupled strategy of the Valence Bond theory. Our very preliminary investigations (Genoni, Franchini *et al.*, 2018) have shown that the determination of XCSC wave functions is quite straightforward. The new technique is efficiently able to capture crystal-field effects intrinsically contained in the experimental structure factors used as external constraints in the XCW calculations, particularly revealing slight but non-negligible differences between the electronic structures in the gas phase and in the solid-state.

In this paper, after presenting for the first time all the theoretical details of the new method, we will also discuss the results of new test calculations to further evaluate the overall performances of the technique. Finally, in the last section, we will draw some general conclusions and we will indicate possible future perspectives and extensions of the proposed strategy.

2. Theory

In this section we will describe the theory at the basis of the new X-ray constrained Spin-Coupled method. In particular, we will focus *i)* on the basic assumptions of the technique, *ii)* on the

presentation of the new wave function *ansatz*, *iii)* on the expression of the Spin-Coupled electron density and *iv)* on the implementation of the new strategy. For the sake of completeness, the detailed mathematical derivation to obtain the analytical expressions of the first and second derivatives of the statistical agreement between theoretical and experimental structure factors amplitudes is given in the final Appendix of the paper.

2.1. Basic assumptions of the method

As in any XCW method ((Jayatilaka, 1998; Jayatilaka & Grimwood, 2001; Grimwood & Jayatilaka, 2001; Bytheway, Grimwood & Jayatilaka, 2002; Bytheway, Grimwood, Figgis *et al.*, 2002; Grimwood *et al.*, 2003; Hudák *et al.*, 2010; Jayatilaka, 2012; Bučinský *et al.*, 2016; Genoni, 2013a; Genoni, 2013b; Dos Santos *et al*., 2014; Genoni & Meyer, 2016; Genoni, 2017; Casati *et al*., 2017), also the new X-ray constrained Spin-Coupled approach works for molecular crystals and assumes them as collections of non-interacting molecular units, which are described by formally identical and symmetry-related wave functions. On the basis of this working hypothesis and of the additional assumption that each non-interacting unit corresponds to a symmetry-unique portion of the crystal unit-cell, the electron density of the crystal unit-cell can be expressed as the sum of the N_m crystal-unit electron densities $\rho_j(\boldsymbol{r})$ related to the reference distribution $\rho_0(\boldsymbol{r})$ through the unit-cell symmetry operations $\{\boldsymbol{Q}_j, \boldsymbol{q}_j\}$:

$$\rho_{cell}(\boldsymbol{r}) = \sum_{j=1}^{N_m} \rho_j(\boldsymbol{r}) = \sum_{j=1}^{N_m} \rho_0\left[\boldsymbol{Q}_j^{-1}(\boldsymbol{r} - \boldsymbol{q}_j)\right] \qquad (1)$$

This equation is exact only provided that $\rho_0(\boldsymbol{r})$ is not obtained by means of an isolated computation on the reference crystal-unit. In the XCW approaches this requirement is satisfied by looking for wave function Ψ_0 associated with electron density $\rho_0(\boldsymbol{r})$ that minimizes the energy of the reference crystal-unit and that, at the same time, reproduces a set of experimental structure factors amplitudes within the limit imposed by the experimental uncertainties. In this way the effects of the surrounding crystal-field are intrinsically taken into account in an effective way, although the XCW computations formally consist in single-molecule computations.

In other words, the new XCSC method and all the XCW techniques consist in determining wave function Ψ_0 of the reference crystal-unit that minimizes the Jayatilaka functional:

$$\begin{aligned} J[\Psi_0] &= \frac{\langle \Psi_0 | \widehat{\mathcal{H}}_0 | \Psi_0 \rangle}{\langle \Psi_0 | \Psi_0 \rangle} + \lambda \left(\chi^2[\Psi_0] - \Delta\right) \\ &= W[\Psi_0] + \lambda \left(\chi^2[\Psi_0] - \Delta\right) \qquad (2), \end{aligned}$$

In equation (2), the first term of the functional is obviously the energy part with $\widehat{\mathcal{H}}_0$ as the non-relativistic Hamiltonian operator for the reference unit, while the second term of the functional is the

part that takes into account the experimental constraints given by X-ray diffraction data, with λ as an external multiplier that is manually adjusted during the calculations and that gives the strength of the experimental constraints, Δ as the desired agreement between theoretical and observed structure factors amplitudes (usually set equal to 1). χ^2 is a measure of the statistical agreement between calculated and experimental values:

$$\chi^2 = \frac{1}{N_r - N_p} \sum_{\boldsymbol{h}} \frac{\left(\eta \left|F_{\boldsymbol{h}}^{calc}\right| - \left|F_{\boldsymbol{h}}^{exp}\right|\right)^2}{\sigma_{\boldsymbol{h}}^2} \qquad (3)$$

with N_r as the number of experimental constraints, N_p as the number of adjustable parameters, $\boldsymbol{h}$ as the triad of Miller indices that characterize the reflection, $\sigma_{\boldsymbol{h}}$ as the experimental error associated with the generic experimental structure factor amplitude $\left|F_{\boldsymbol{h}}^{exp}\right|$ and η as an overall $\boldsymbol{h}$-independent scale-factor that multiplies each computed structure factor amplitude $\left|F_{\boldsymbol{h}}^{calc}\right|$ and that is obtained through minimization of the χ^2 value.

For the sake of completeness, considering the basic assumptions of the XCW philosophy and the fact that structure factors are Fourier transforms of the unit-cell electron density, we remind that the calculated structure factors can be computed like this:

$$F_{\boldsymbol{h}}^{calc} = Tr[\boldsymbol{D}_0 \, \boldsymbol{I}_{\boldsymbol{h}}] \qquad (4)$$

with $\boldsymbol{D}_0$ as the one-particle density matrix associated with wavefunction Ψ_0 for the reference crystal-unit and $\boldsymbol{I}_{\boldsymbol{h}}$ as the matrix of the Fourier-transform integrals of the basis functions products summed over the N_m equivalent unit-cell sites, namely

$$[\,\boldsymbol{I}_{\boldsymbol{h}}]_{\mu\upsilon} = \sum_{j=1}^{N_m} e^{i2\pi\, \boldsymbol{q}_j \cdot (\boldsymbol{B}\boldsymbol{h})}\, T_{\mu\upsilon}\left[\boldsymbol{B}^{-1}\boldsymbol{Q}_j^T\boldsymbol{B}\boldsymbol{h};\ \boldsymbol{U}^{\mu}, \boldsymbol{U}^{\nu}\right] \int d\boldsymbol{r}\ \chi_{\mu}(\boldsymbol{r})\, \chi_{\upsilon}(\boldsymbol{r})\, e^{i2\pi\,(\boldsymbol{Q}_j \boldsymbol{r}) \cdot (\boldsymbol{B}\boldsymbol{h})} \qquad (5)$$

In equation (5), $\boldsymbol{B}$ is the reciprocal lattice matrix and $T_{\mu\upsilon}\left[\boldsymbol{B}^{-1}\boldsymbol{Q}_j^T\boldsymbol{B}\boldsymbol{h};\ \boldsymbol{U}^{\mu}, \boldsymbol{U}^{\nu}\right]$ is a term that accounts for the influence of the thermal motion on the electron density and that, in our new XCSC technique, has been evaluated following the thermal smearing approach proposed by Stewart (Stewart, 1969). It is worth noting that this term parametrically depends on the symmetric matrices $\boldsymbol{U}^{\mu}$ and $\boldsymbol{U}^{\nu}$ of the Anisotropic Displacement Parameters (ADPs) of the atoms on which basis functions $\chi_{\mu}(\boldsymbol{r})$ and $\chi_{\upsilon}(\boldsymbol{r})$ are centered. As in any X-ray constrained wavefunction fitting calculation, these ADPs are read as input parameters and never optimized during the computations.

2.2. The Spin-Coupled wave function *ansatz*

In the novel X-ray constrained Spin-Coupled method, the analytical form for wave function Ψ_0 associated with the reference crystal-unit is the one of the traditional Spin-Coupled wave function for a system of N electrons in the spin-state (S, M):

$$\Psi_0 = \mathcal{N}\,\Psi_0^{SC} = \mathcal{N}\sum_{k=1}^{f_S^{N_v}} c_{S,k}\,\psi_{S,M;k}^{N} =$$

$$= \mathcal{N}\sum_{k=1}^{f_S^{N_v}} c_{S,k}\;\hat{\mathcal{A}}\left(\phi_1^c\,\bar{\phi}_1^c \ldots \phi_j^c\,\bar{\phi}_j^c \ldots \phi_{N_1}^c\,\bar{\phi}_{N_1}^c\,\boldsymbol{\varphi}_{\mathrm{v}}\,\Theta_{S,M;k}^{N_v}\right) \quad (6)$$

where S and M are the quantum numbers associated with the spin operators $\hat{S}^2$ and $\hat{S}_z$, respectively, $\mathcal{N}$ is the normalization constant, $f_S^{N_v}$ is the number of linearly independent spin-eigenfunctions $\{\Theta_{S,M;k}^{N_v}\}$ and, equivalently, of linearly independent Spin-Coupled structures $\{\psi_{S,M;k}^{N}\}$ with weights given by the spin-coupling coefficients $\{c_{S,k}\}$, and $\hat{\mathcal{A}}$ is the antisymmetrizer defined as:

$$\hat{\mathcal{A}} = \frac{1}{\sqrt{N!}}\sum_{\hat{\mathcal{P}}\in S_N}(-1)^p\;\hat{\mathcal{P}} \qquad (7)$$

with $\hat{\mathcal{P}}$ as a permutation operator belonging to the symmetric group S_N and with parity $(-1)^p$. Furthermore, $\{\phi_i^c\}_{i=1}^{N_1}$ is the set of frozen, doubly occupied "core orbitals" that can be preliminarily obtained by means of unconstrained Hartree-Fock or X-ray constrained Hartree-Fock calculations and that describe the subset of $2N_1$ core (or inactive) electrons, while $\boldsymbol{\varphi}_{\mathrm{v}}$ is the product of the N_v "Spin-Coupled orbitals"

$$\boldsymbol{\varphi}_{\mathrm{v}}\left(\boldsymbol{r}_1, \boldsymbol{r}_2, \ldots \boldsymbol{r}_{N_v}\right) = \varphi_1(\boldsymbol{r}_1)\,\varphi_2(\boldsymbol{r}_2)\ldots\,\varphi_{N_v}(\boldsymbol{r}_{N_v}) \qquad (8)$$

that describe the N_v valence (or active) electrons. As in every SC calculations, these are the only electrons that are really treated at Spin-Coupled level in order to reduce the computational cost. The "core orbitals" are constructed orthonormal among each other and orthogonal to the "Spin-Coupled orbitals", on which, on the contrary, no orthogonality constraints are imposed:

$$\begin{cases}\langle\phi_i^c|\phi_j^c\rangle = \delta_{ij}\\ \langle\phi_i^c|\varphi_j\rangle = 0\\ \langle\varphi_i|\varphi_j\rangle = s_{ij}\end{cases} \qquad (9)$$

Here it is worth noting that, since both unconstrained and X-ray constrained Hartree-Fock orbitals are generally delocalized over all the systems under examination, they are usually localized by means of traditional *a posteriori* techniques (Boys, 1969; Foster & Boys, 1969; Edmiston & Ruedenberg, 1963; Edmiston & Ruedenberg, 1965; Pipek & Mezey, 1989) to select which of them have to be used to describe the core (inactive) electrons. As a consequence, the "core orbitals" are automatically orthonormal among each other, while, to guarantee the orthogonality between the "core orbitals" and the Spin-Coupled orbitals, the latter are expanded on the set of the remaining localized occupied

molecular orbitals (namely, those non-selected as "core orbitals") and of all the virtual (Hartree-Fock or X-ray constrained Hartree-Fock) molecular orbitals, namely:

$$\varphi_i(\boldsymbol{r}) = \sum_{\mu=N_1+1}^{M} C_{\mu i}\, \phi_\mu^{(XC)HF}(\boldsymbol{r}) \qquad (10),$$

where *M* is the size of the adopted basis-set (i.e., the number of atomic basis functions initially used to perform the preliminary Hartree-Fock or X-ray constrained Hartree-Fock calculation).

Due to the non-orthogonality of the SC orbitals, also the Spin-Coupled structures in equation (6) are non-orthogonal. Therefore, the spin-coupling coefficients $\{c_{S,k}\}$ do not directly give the weights of the corresponding structures $\{\psi_{S,M;k}^N\}$. One of the possible ways of obtaining the real weights is given by the Chirgwin-Coulson coefficients (Chirgwin & Coulson, 1950), which have been used in this work and are defined like this:

$$w_{S,k} = \left|c_{S,k}\right|^2 + \sum_{j\neq k} c_{S,k}\, c_{S,j}\, S_{kj} \quad (11)$$

where S_{kj} is the overlap integral between Spin-Coupled structures $\psi_{S,M;k}^N$ and $\psi_{S,M;j}^N$.

To complete the overview on the SC wave function *ansatz*, it is also important to note that each generic spin-eigenfunction can be expressed as linear combination of spin primitive functions, namely

$$\Theta_{S,M;k}^{N_v} = \sum_{i=1}^{N_d} d_{i,k}^S\, \vartheta_i \qquad (12)$$

where $N_d = \binom{N_v}{N_\alpha} = \binom{N_v}{N_\beta}$, with N_α and N_β as the number of spin functions α and β in the generic spin primitive function, respectively. The values of the coefficients $\{d_{i,k}^S\}$ depend on the adopted basis to describe the spin-space. In our work we have chosen the one constituted of Rumer spin-eigenfunctions (Simonetta *et al.*, 1968) and, for this reason, $\{d_{i,k}^S\}$ can be only equal to 0 and ±1. Now, if we introduce equation (12) into (6), the Spin-Coupled wave function *ansatz* can be also rewritten like this:

$$\Psi_0 = \mathcal{N} \sum_{i=1}^{N_d} b_{S,i}\, \hat{\mathcal{A}}\left(\phi_1^c\, \bar{\phi}_1^c \ldots \phi_j^c\, \bar{\phi}_j^c \ldots \phi_{N_1}^c\, \bar{\phi}_{N_1}^c\, \boldsymbol{\varphi}_{\mathrm{v}}\, \vartheta_i\right) \quad (13)$$

where

$$b_{S,i} = \sum_{k=1}^{f_S^{N_v}} c_{S,k}\, d_{i,k}^S \qquad (14)$$

Since the generic spin primitive function ϑ_i is a product of N_v spin functions α and β, product $\boldsymbol{\varphi}_{\mathrm{v}}\,\vartheta_i$ in equation (13) is actually a product of spinorbitals, namely

$$\boldsymbol{\varphi}_{\mathrm{v}}\,\vartheta_i = \varphi_1\,\varphi_2 \ldots \varphi_{N_v}\vartheta_i = \varphi_1^i\,\varphi_2^i \ldots \varphi_{N_v}^i \qquad (15)$$

where $\varphi_j^i = \varphi_j\,\omega_j^i$ with ω_j^i as the *j*-th spin function (α or β) of the *i*-th spin primitive function ϑ_i. Therefore, in equation (13), the antisymmetrizer applied to the spinorbitals product generates a Slater determinant and, consequently, the Spin-Coupled *ansatz* becomes:

$$\Psi_0 = \mathcal{N}\sum_{i=1}^{N_d}\frac{b_{S,i}}{\sqrt{N!}}\left|\phi_1^c\,\bar{\phi}_1^c \ldots \phi_j^c\,\bar{\phi}_j^c \ldots \phi_{N_1}^c\,\bar{\phi}_{N_1}^c\,\varphi_1^i\,\varphi_2^i \ldots \varphi_{N_v}^i\right| = \mathcal{N}\sum_{i=1}^{N_d} b_{S,i}\,\Omega_i \quad (16),$$

namely, it can be written as a linear combination of Slater determinants $\{\Omega_i\}$. Furthermore, exploiting equation (16) and bearing in mind the Löwdin rules (Löwdin, 1955; McWeeny, 1992) for the computation of overlap integrals and matrix elements between Slater determinants constructed with non-orthogonal orbitals, it is easy to show that

$$\mathcal{N} = \mathfrak{D}^{-\frac{1}{2}} \quad (17)$$

where $\mathfrak{D}$ is the zero-th order supercofactor given by

$$\mathfrak{D} = \sum_{i,j=1}^{N_d} b_{S,i}\,b_{S,j}\,\det\left[\boldsymbol{O_{ij}}\right] \quad (18)$$

with $\boldsymbol{O_{ij}}$ as the matrix of the overlap integrals between the spinorbitals of Slater determinants Ω_i and Ω_j appearing in equation (16). Therefore, the wave function *ansatz* for the reference crystal-unit can be finally rewritten in this way:

$$\Psi_0 = \mathfrak{D}^{-\frac{1}{2}}\sum_{i=1}^{N_d}\frac{b_{S,i}}{\sqrt{N!}}\left|\phi_1^c\,\bar{\phi}_1^c \ldots \phi_j^c\,\bar{\phi}_j^c \ldots \phi_{N_1}^c\,\bar{\phi}_{N_1}^c\,\varphi_1^i\,\varphi_2^i \ldots \varphi_{N_v}^i\right| = \mathfrak{D}^{-\frac{1}{2}}\sum_{i=1}^{N_d} b_{S,i}\,\Omega_i \quad (19)$$

2.3. The Spin-Coupled electron density

Exploiting wave function Ψ_0, the electron density $\rho_0(\boldsymbol{r})$ of the reference crystal-unit can be simply obtained like this:

$$\rho_0(\boldsymbol{r}) = \int_{\boldsymbol{x}_1=\boldsymbol{x}} d\omega_1\,d\boldsymbol{x}_2\,d\boldsymbol{x}_3 \ldots d\boldsymbol{x}_N\,\Psi_0(\boldsymbol{x}_1,\boldsymbol{x}_2,\ldots,\boldsymbol{x}_N)\,\Psi_0^*(\boldsymbol{x}_1,\boldsymbol{x}_2,\ldots,\boldsymbol{x}_N) \quad (20)$$

Substituting (19) in (20) and using again the Löwdin rules, we obtain:

$$\rho_0(\boldsymbol{r}) = \rho_{core}(\boldsymbol{r}) + \frac{\rho_{SC}(\boldsymbol{r})}{\mathfrak{D}} = 2\sum_{t=1}^{N_1}|\phi_t^c(\boldsymbol{r})|^2 + \frac{1}{\mathfrak{D}}\sum_{t,u=1}^{N_v}\varphi_t(\boldsymbol{r})\,\varphi_u(\boldsymbol{r})\,\mathfrak{D}(t|u) \quad (21)$$

where $\mathfrak{D}(t|u)$ is the fist-order supercofactor, which is defined like this:

$$\mathfrak{D}(t|u) = \sum_{i,j=1}^{N_d} b_{S,i}\, b_{S,j}\; I_{tu}^{ij}\; (-1)^{t+u}\; \det\left[\boldsymbol{O_{ij}}(t|u)\right] \qquad (22)$$

with I_{tu}^{ij} as the spin-integral between the spin-part of the *t*-th spinorbital of the *i*-th Slater determinant and the spin-part of the *u*-th spinorbital of the *j*-th Slater determinant, and $\boldsymbol{O_{ij}}(t|u)$ as the (*N*-1)-th order matrix obtained by deleting row *t* and column *u* of matrix $\boldsymbol{O_{ij}}$, which was defined above (the more general definition of *r*-th order supercofactors and the main properties of the different kind of supercofactors are given in Appendix A1).

2.4. Implementation of the XCSC technique

Considering the analytical form of the new wave function *ansatz* (see particularly equation (6)) and of the active SC orbitals (see equation (10)), the new X-ray constrained Spin-Coupled method consists in determining the coefficients $\{C_{\mu i}\}$ of the Spin-Coupled orbitals expansions and the spin-coupling coefficients $\{c_{S,k}\}$ that minimize the Jayatilaka functional shown in equation (2), which can be re-expressed in this way to stress the dependence of the functional on the coefficients that must be determined:

$$J\left[\{C_{\mu i}\},\{c_{S,k}\}\right] = W\left[\{C_{\mu i}\},\{c_{S,k}\}\right] + \lambda\left(\chi^2\left[\{C_{\mu i}\},\{c_{S,k}\}\right] - \Delta\right) \qquad (23)$$

To accomplish this task, we started from a working Spin-Coupled program (Cooper *et al.*, 1993) where we have implemented a Newton-Raphson procedure based on the "quadratic hill climbing" algorithm proposed by Goldfield and coworkers (Goldfield *et al.*, 1966). The algorithm requires the computation of analytical first and second derivatives of functional (23) with respect to Spin-Coupled orbitals and spin-coupling coefficients, whose mathematical derivations and expressions are shown in Appendix A2. Convergence is reached when the norm of the functional gradient is lower than $1 \cdot 10^{-6}$ and all the Hessian eigenvalues are positive.

3. Test Calculations

3.1. Preliminary information

To better assess the performances of the new X-ray constrained Spin-Coupled method, we have exploited the high-resolution X-ray diffraction data ($sin\theta/\lambda = 1.08$ Å^{-1}) for salicylic acid collected at 90 K by Munshi and Guru-Row (Munshi & Guru-Row, 2006). In particular, the molecular geometry obtained from the X-ray diffraction experiment (see Figure 1) has been exploited to carry out calculations at Restricted Hartree-Fock (RHF), X-ray constrained Restricted Hartree-Fock (XC-

RHF), Spin-Coupled (SC) and X-ray constrained Spin-Coupled (XCSC) levels. Furthermore, since one of the goals of our investigation was also to evaluate how the results obtained through the new XCSC strategy change in function of the adopted basis-sets, we have performed all the above mentioned computations using the 6-31G, 6-311G, 6-31G(d) and 6-311G(d) sets of basis functions.

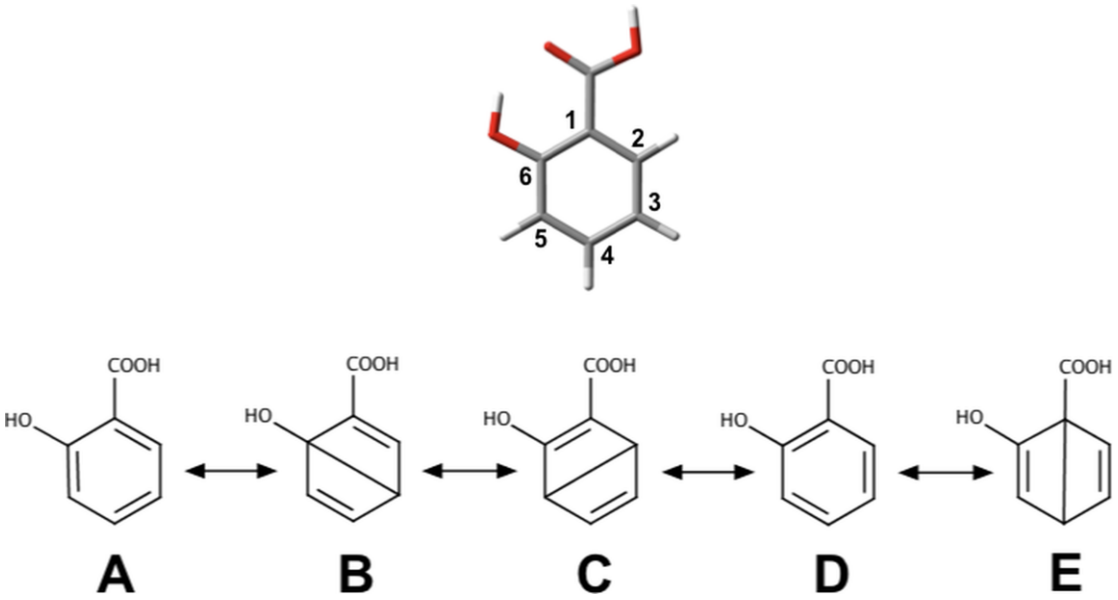

Figure 1 X-ray crystal structure of salicylic acid with labels for the carbon atoms of the aromatic ring and Spin-Coupled resonance structures taken into account in the unconstrained and X-ray constrained Spin-Coupled calculations (A, D: Kekulé resonance structures; B, C and E: Dewar resonance structures).

For all the unconstrained and X-ray constrained Spin-Coupled calculations, only the 6 π electrons of the aromatic ring have been considered as valence (active) electrons and, consequently, fully treated at spin-coupled level (see wave function *ansatz* (6)). The other core (inactive) electrons have been described by frozen doubly occupied "core" molecular orbitals and always kept orthogonal to the (active) spin-coupled space (see equations (9) and following paragraph in the Theory Section). In particular, two kinds of core orbitals have been considered for our SC and XCSC computations. In one case (and in analogy with the original version of the XCSC approach (Genoni, Franchini *et al.*, 2018)) we have used unconstrained RHF molecular orbitals, which allowed us to perform calculations that will be hereafter labeled as SC.0 and XCSC.0. In the other case we have used molecular orbitals that resulted from preliminary XC-RHF computations and that enabled us to carry out new types of Spin-Coupled and X-ray constrained Spin-Coupled calculations. They will be labeled as SC.1 and XCSC.1, respectively. As we will discuss hereinafter, this represents an important step forward compared to the previous version of the X-ray constrained Spin-Coupled strategy (Genoni, Franchini *et al.*, 2018) because also the inactive part of the spin-coupled wave function intrinsically takes into account the effect of the experimental diffraction data, thus leading to a more balanced description of the electronic structure.

For the sake of completeness, it is also worth noting that, due to their intrinsic delocalized nature, the RHF and XC-RHF occupied molecular orbitals have been preliminarily localized exploiting the Pipek-Mezey localization technique (Pipek & Mezey, 1989) to determine which of them to freeze for the description of the inactive electrons and which of them to use in the expansion of the active Spin-Coupled orbitals (see equation (10)).

Furthermore, since for a system of N_v active electrons in the spin-state (S, M) the number of possible spin-coupling modes are given by

$$f_S^{N_v} = \frac{(2S+1)N_v!}{\left(\frac{1}{2}N_v + S + 1\right)!\,\left(\frac{1}{2}N_v - S\right)!} \qquad (24)$$

and since in our investigations we treated only singlet states, in all our SC and XCSC calculations we have considered 5 spin-coupled structures (see again equation (6)), which correspond to the 5 resonance structures depicted in Figure 1, where structures A and D correspond to the traditional Kekulé resonance structures, while B, C and E are the Dewar ones.

Concerning the XC-RHF and all types of XCSC calculations we also exploited the lattice parameters (namely, unit-cell lengths and angles), ADPs and structure factors amplitudes deposited with the considered crystallographic structures. Only structure factor amplitudes characterized by $\left|F_{\boldsymbol{h}}^{exp}\right| > 3\,\sigma_{\boldsymbol{h}}$ were considered in the computations, which resulted in the selection of 6157 unique reflections. Furthermore, all the X-ray constrained computations (i.e., XC-RHF, XCSC.0 and XCSC.1) were carried out by gradually increasing the value of the external multiplier λ from 0 (unconstrained computations) and, as we will show below in more details, to halt the XCSC calculations we have proposed and adopted a novel termination criterion based on the sign of the second derivative of χ^2 with respect to λ.

While unconstrained RHF and XC-RHF computations were carried out using the quantum chemistry package Gaussian09 (Frisch *et al.*, 2009) and the quantum crystallography software TONTO (Jayatilaka & Grimwood, 2003), respectively, all kind of XCSC calculations were performed by exploiting our in-house program mentioned in the Theory section.

To evaluate the general capabilities of the XCSC technique, in the next subsections we will show the changes in the χ^2 statistical agreements, in the weights of the resonance structures and in the Spin-Coupled orbitals when the experimental X-ray diffraction data are taken into account in the Spin-Coupled calculations. Furthermore, we will also present how these changes are influenced by the adopted basis-set.

For the sake of clarity, we will start discussing the results of the SC.0 and XCSC.0 computations. Afterwards we will focus on the outcomes of the SC.1 and XCSC.1 calculations. Finally, in the last part of this section, we will also show the effects of accounting for the experimental structure factors

on the global electron density distributions, both by visual inspection of density differences and through the evaluation of similarity indexes between the obtained electron densities.

3.2. Calculations based on unconstrained RHF molecular orbitals

In the first validation tests, both Spin-Coupled and X-ray constrained Spin-Coupled calculations were performed using the unconstrained RHF molecular orbitals to describe the inactive electrons. The χ^2 and energy values resulting from these computations are reported in Table 1 ("RHF MOs" column), where it is easy to observe that, for all the considered basis-sets, the statistical agreement with the experimental data always slightly improves when the XCSC.0 computations are performed. Furthermore, as one should expect, the XCSC.0 description improves (always in terms of agreement with the experimental data) when larger and more flexible basis-sets are taken into account, with the χ^2 value decreasing from 13.51 (6-31G basis-set) to 8.07 (6-311G(d) basis-set). Nevertheless, it is also evident that, despite the application of the X-ray constrained Spin-Coupled approach, for all the basis sets, the values of the statistical agreements remain quite high and close to those associated with the unconstrained RHF and SC.0 computations. The reason is that, in all the XCSC.0 calculations, only 6 electrons were actually treated at XCSC level, while the remaining ones (namely, the inactive electrons) were described by doubly occupied molecular orbitals that resulted from unconstrained RHF computations and that, consequently, cannot take into account the effect of the experimental X-ray diffraction data. To reach lower values of the χ^2 statistical agreements by means of XCSC calculations, the only possibility is to exploit XC-RHF molecular orbitals to describe the core electrons. This has been actually done through the SC.1 and XCSC.1 computations, which will be discussed in the next subsection. For the sake of completeness, in Table 1 it is also possible to notice that, for all the basis-sets, the energies associated with the XCSC.0 wave functions are higher than those corresponding to the SC.0 wave functions. As already discussed in our preliminary work on the XCSC method (Genoni, Franchini *et al.*, 2018), this arises from the fact that in every X-ray constrained wave function technique, the determination of the "experimental" wave function is accomplished without introducing new variational parameters. Consequently, the resulting spin-coupled orbitals and the spin-coupling coefficients represent a minimum point for the Jayatilaka functional (see equation (23)), but not for the energy of the system.

Table 1 χ^2 statistical agreement and energy values for all the unconstrained and X-ray constrained calculations performed on salicylic acid. The value of the external parameter λ is also reported for X-ray constrained calculations.

Method & Basis-Set	Calculations with RHF MOs [a]			Calculations with XC-RHF MOs [b]		
	λ_{max}	χ^2	Energy (E_h)	λ_{max}	χ^2	Energy (E_h)
6-31G						
RHF / XC-RHF		14.05	-492.975931	0.100	5.66	-492.817879
SC.0 / SC.1		14.01	-493.037815		5.87	-492.884062
XCSC.0 / XCSC.1	0.100	13.51	-493.020372	0.326	5.58	-492.861463
6-311G						
RHF / XC-RHF		13.70	-493.088826	0.105	4.93	-492.919497
SC.0 / SC.1		13.66	-493.150622		5.14	-492.984446
XCSC.0 / XCSC.1	0.105	13.08	-493.129330	0.315	4.86	-492.961320
6-31G(d)						
RHF / XC-RHF		9.34	-493.179441	0.150	3.59	-493.053881
SC.0 / SC.1		9.14	-493.238706		3.74	-493.120653
XCSC.0 / XCSC.1	0.150	8.56	-493.207299	0.610	3.52	-493.096062
6-311G(d)						
RHF / XC-RHF		8.85	-493.285839	0.140	3.49	-493.172468
SC.0 / SC.1		8.67	-493.344578		3.63	-493.237150
XCSC.0 / XCSC.1	0.140	8.07	-493.314518	0.640	3.41	-493.209195

[a] Results for RHF, SC.0 and XC.0 calculations

[b] Results for XC-RHF, SC.1 and XCSC.1 calculations

As already anticipated, for the termination of the XCSC calculations performed in this study we have adopted a new criterion. This point deserves to be discussed in more details because, despite many suggestions have been proposed over the years, the determination of the exact value of λ at which stopping the X-ray constrained computations is still an open and debated problem. The new criterion simply consists in halting the X-ray constrained calculations when the curvature of the typical graph of χ^2 in function of λ changes, namely when the second derivative $\partial^2\chi^2/\partial\lambda^2$ becomes negative (inflection point). In fact, by plotting χ^2 against λ for all the XCSC.0 calculations, we easily observed clear changes in the curvature of the graphs (see Figures S1-S4 in the Supporting Information) and, above all, we have also noted that the XCSC computations generally stopped converging few steps after the inflection point. This observation was further corroborated by the fact that, for λ values only

slightly larger than the detected inflection points, even the more traditional XC-RHF computations showed instabilities and difficulties in reaching convergence. In other words, the second derivative $\partial^2\chi^2/\partial\lambda^2$ can be considered as a useful descriptor to detect the onset of instability in the X-ray constrained wave function procedure. Although at the moment it is only based on empirical observations, the new criterion seems quite promising and robust. In our opinion, it will deserve further investigations in the future by means of more extensive tests and statistical analyses, also applying it to traditional X-ray constrained calculations as the XC-RHF ones. However, it is also worth pointing out that the use of the adopted termination criterion does not invalidate the new X-ray constrained Spin-Coupled method and the assessment of its performances discussed in the present paper.

In the Introduction we have also mentioned that one of the novelties introduced through the new X-ray constrained Spin-Coupled techniques is the possibility of extracting resonance structures weights for the systems under examination directly from the collected experimental diffraction data. In Table 2, we have reported the Chirgwin-Coulson weights corresponding to resonance structures of salicylic acid in its singlet state as obtained from the SC.0 and XCSC.0 calculations. The trend is generally analogous for almost all the basis-sets. Concerning Kekulé structures A and D, we can see that, while the weight of the former slightly increases in almost all the cases when experimental data are taken into account (the only exception is for basis-set 6-31G(d)), the importance of the latter always decreases, with the largest variations observed for basis-sets with polarization functions (Δ = -2.5 and Δ = -3.3 for basis-sets 6-31G(d) and 6-311G(d), respectively). Considering the remaining Dewar structures (namely, structures B, C and E), we can observe that structure B loses its weight when X-ray data are included in the calculations and, interestingly, all the X-ray constrained computations provided very close values. On the contrary, structure C is characterized by larger weights in the XCSC.0 calculations and, also in this case, the resulting values are very similar among them. Structure E is the only one for which the trends are different for basis-sets with and without polarization functions, with its importance that decreases for basis-sets 6-31G and 6-311G and that, conversely, increases for basis-sets 6-31G(d) and 6-311G(d).

Table 2 Chirgwin-Coulson weights (in %) of the salicylic acid resonance structures resulting from the SC.0 and XCSC.0 calculations for all the considered basis-sets.

Structures	6-31G		6-311G		6-31G(d)		6-311G(d)	
	SC.0	XCSC.0	SC.0	XCSC.0	SC.0	XCSC.0	SC.0	XCSC.0
A	16.6	17.2	16.6	18.4	15.7	15.7	15.7	16.9
B	8.8	7.6	8.7	7.6	9.3	7.5	9.1	7.8
C	9.5	12.2	9.4	12.3	9.7	12.9	9.6	12.4
D	54.7	52.9	55.0	52.6	53.8	51.3	54.3	51.0
E	10.4	10.1	10.2	9.1	11.5	12.6	11.3	11.9

To complete the analysis of the results obtained from the XCSC.0 calculations, we have finally decided to focus on the Spin-Coupled orbitals for the 6 active electrons obtained from the X-ray constrained Spin-Coupled calculations performed on salicylic acid (see Figure 2). In particular, we analyzed their variations with respect to the corresponding unconstrained SC.0 orbitals, namely we evaluated the effect of the experimental diffraction data on the spin-coupled orbitals. From Figure 3 it is clear that the orbitals variations resulting from the calculations with basis-sets without polarization functions are very similar between each other. Likewise, also the orbitals variations obtained from calculations with basis-sets including polarization functions present a high degree of similarity.

Through a more detailed inspection, it is also possible to see that, for orbitals φ_2, φ_3 and φ_4, when basis-sets 6-31G and 6-311G are used, the variations mainly consist in a slight delocalization from the atoms on which the unconstrained SC.0 orbitals are mainly localized to the neighbor atoms. Conversely, for the same orbitals, when basis-sets 6-31G(d) and 6-311G(d) are exploited, we have an opposite trend, with the spin-coupled orbitals that tend to further localize on the central atoms. This opposite behavior can be ascribed to the effect of the experimental diffraction data. In fact, in absence of polarization functions, the SC.0 orbitals φ_2, φ_3 and φ_4 are less polarized towards the neighbor atoms and the effect of the X-ray diffraction data in the XCSC.0 computations is a delocalization over the neighbor carbon atoms. On the contrary, in presence of polarization functions, the starting SC.0 orbitals are already polarized towards the other atoms, probably at a higher level than the one compatible with the collected experimental data. Therefore, accounting for the X-ray diffraction data in the XCSC.0 calculations, the polarization of the orbitals is tempered mainly through a shift of the electronic clouds from the bonding regions to the central carbon atom (especially for orbitals φ_3 and φ_4).

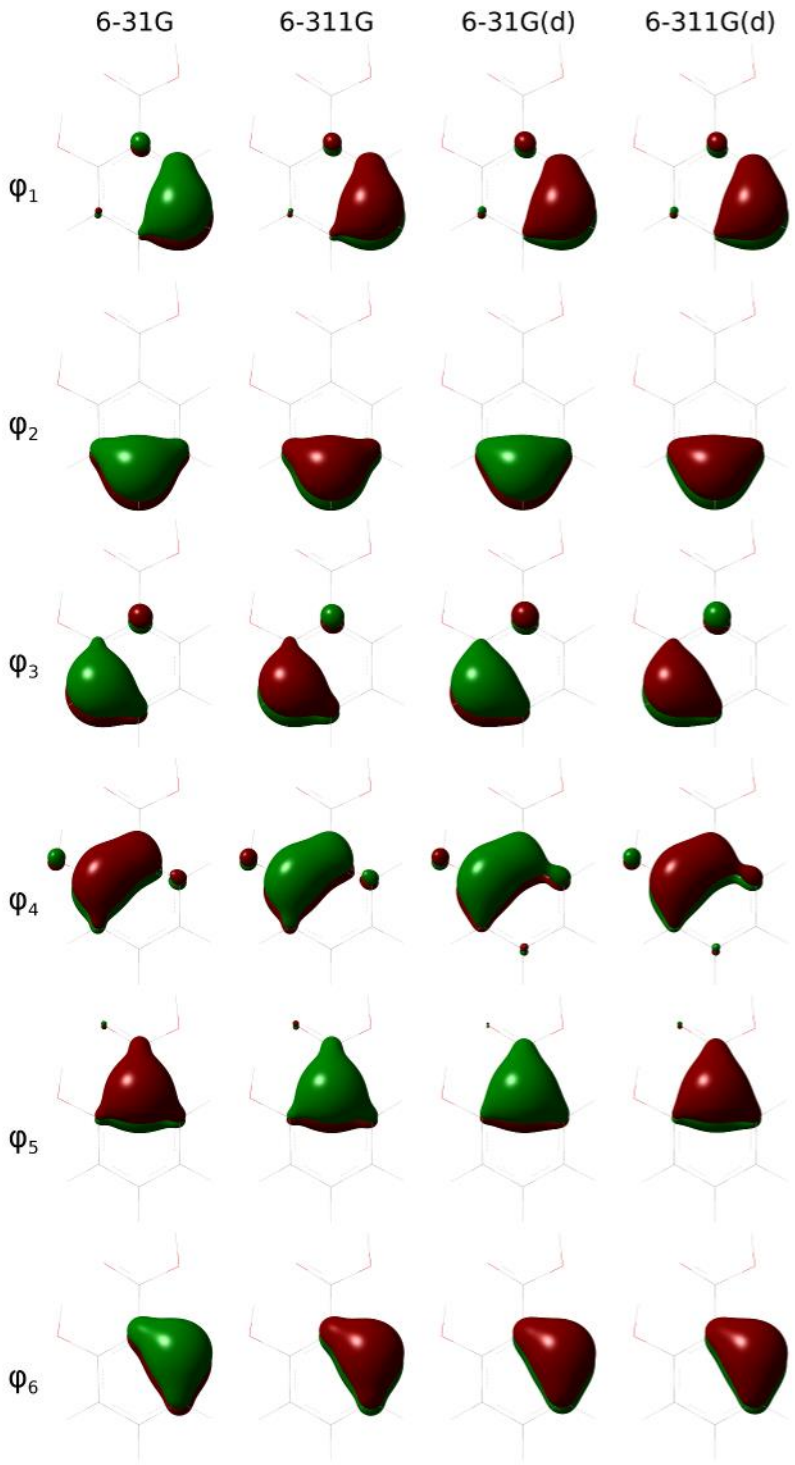

Figure 2 Three-dimensional plots of the unconstrained SC.0 Spin-Coupled orbitals (0.06 e/bohr^3 isosurfaces are plotted). The unconstrained SC.1 Spin-Coupled orbitals have analogous shapes.

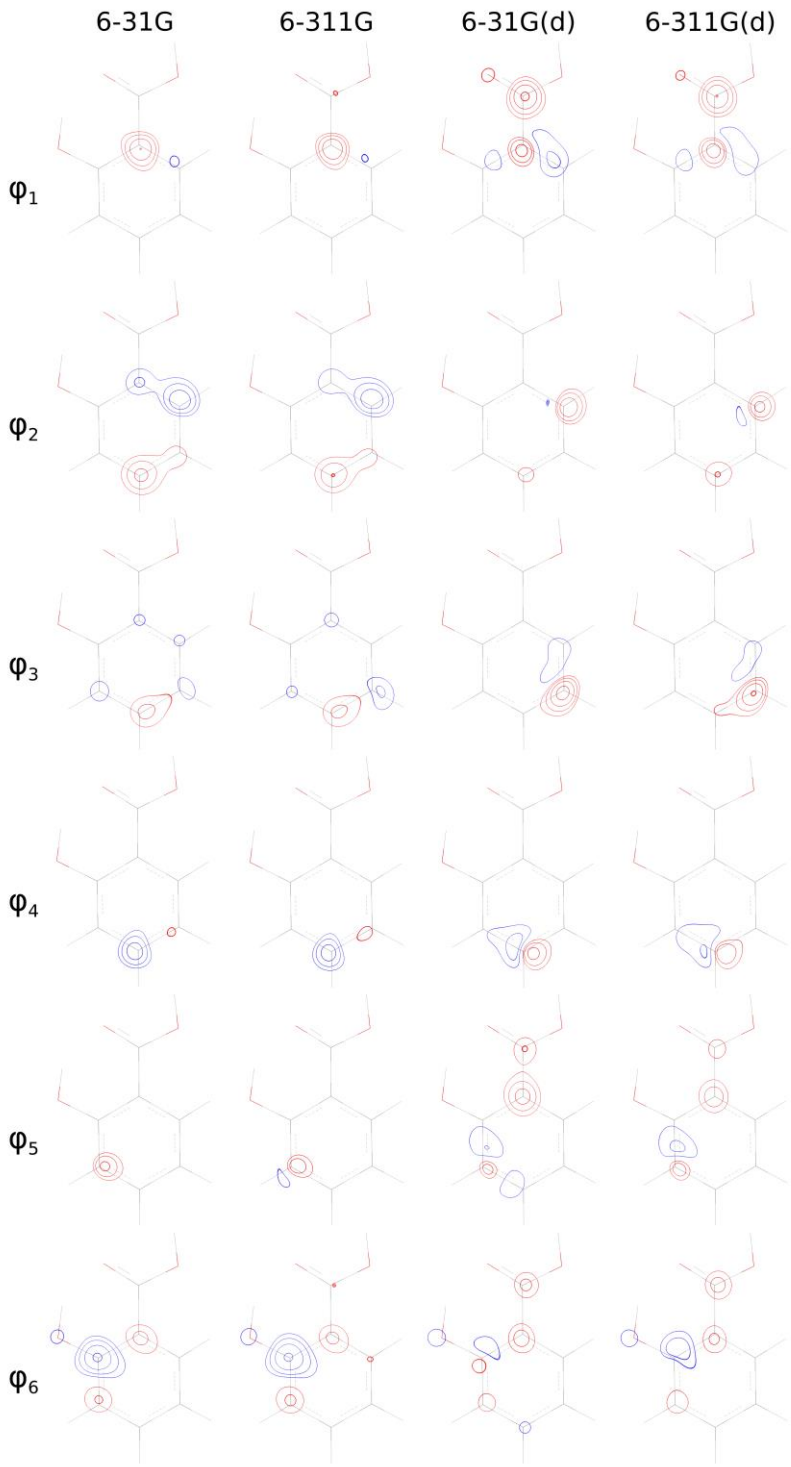

Figure 3 Two-dimensional plots of the differences between the square moduli of the XCSC.0 and SC.0 Spin-Coupled orbitals for all the considered basis-sets. The contours are drawn at $\pm 1 \cdot 10^{-3}$ e/bohr^3 and at $\pm 2, 4, 8 \cdot 10^{n}$ e/bohr^3 (with n as an integer ranging from -3 to 0) in a plane parallel to and 0.5 Å above the aromatic ring. Red and blue contours indicate positive and negative values, respectively.

For orbitals φ_1, φ_5 and φ_6, the variations within the aromatic ring are quite similar for all the basis-sets aside from the use of polarization functions in the calculations, even if for basis-sets 6-31G(d) and 6-311G(d) these orbitals delocalize towards the carboxylic group when experimental data are taken into account. For orbitals φ_1 and φ_5 it is possible to notice stronger localizations on the carbon atoms on which the spin-coupled orbitals are mainly localized, with shifts of electron density from the neighbor bonding regions that are more pronounced when polarization functions are used. For orbital φ_6 the variation is more convoluted, with a shift of the electronic cloud mainly from the carbon atom bearing the hydroxyl group to the neighbor atoms. In this case the effect is more evident when basis-sets without polarization functions are used, while it is barely sketched with basis-sets 6-31G(d) and 6-311G(d).

3.3. Calculations based on X-ray constrained RHF molecular orbitals

To improve the description provided by the XCSC.0 calculations, we have afterwards performed a new series of X-ray constrained Spin-Coupled computations (XCSC.1 computations) that exploit XC-RHF molecular orbitals to describe the inactive electrons.

Energy and χ^2 values resulting from these calculations are reported in Table 1 ("XC-RHF MOs" column) where it is immediately evident that the statistical agreements associated with the XCSC.1 wave functions are significantly better than the corresponding XCSC.0 ones. Furthermore, as for the SC.0 and XCSC.0 computations, the χ^2 values associated with the XCSC.1 wave functions are always slightly lower than the unconstrained SC.1 values and, as expected, the statistical agreement with the experimental data improves as richer basis-sets are used, with χ^2 decreasing from 5.58 (6-31G basis-set) to 3.41 (6-311G(d) basis-set). Finally, it is worth noting that, in Table 1, the SC.1 χ^2 values are always larger than the XC-RHF ones, which is in contrast with the results obtained from the calculations with unconstrained RHF molecular orbitals. This different behavior can be explained considering that, in the SC.1 computations, only the core orbitals fully take into account the effect of the experimental data, while the spin-coupled ones (which describe the active electrons) are obtained by simply minimizing the energy of the system and not the Jayatilaka functional. Conversely, in the XC-RHF computation all the molecular orbitals result from the minimization of the functional given by Equation (2) and, for this reason, they completely take into account the influence of the X-ray diffraction data. Anyway, as seen above, the SC.1 descriptions are improved by carrying out the XCSC.1 calculations, through which also the active spin-coupled orbitals are optimized by fully considering the constraints of the experimental data.

Concerning the termination of the XCSC.1 computations, we have used again the criterion based on the sign of second derivative $\partial^2\chi^2/\partial\lambda^2$. In these cases, the curves representing the trend of χ^2 in function of λ are much more regular and smoother than those associated with the XCSC.0

calculations, but they are anyway characterized by inflection points (see Figures S5-S8 in the Supporting Information), after which convergence rapidly becomes difficult or impossible.

As in the previous subsection, in Table 3 we report the obtained Chirgwin-Coulson weights for the resonance structures of salicylic acid, as obtained from the SC.1 and XCSC.1 calculations. The trends are almost identical for all the basis-sets and are generally analogous to those resulting from the calculations based on unconstrained RHF molecular orbitals. Moreover, despite unavoidable discrepancies in the absolute values, the results show quite consistently how the resonance structure weights change when the experimental X-ray diffraction data are used as external constraints in the computations. In particular, Kekulé resonance structure A gains weight when X-ray data are taken into account, with the only exception of basis-set 6-31G, for which a 0.3 drop has been observed. Conversely, the other Kekulé structure (namely, structure D) consistently loses its importance for all the considered basis-sets, also with significant reductions compared to the SC.1 values (e.g., $\Delta = -4.3$ for basis-set 6-311G(d)). Concerning the Dewar resonance structures, when experimental constraints are introduced in the calculations, the weight of B slightly decreases, while both C and E acquire importance, with the only exception of the 6-311G(d) calculations, for which the Chirgwin-Coulson coefficient for structure E decreases from 11.3 to 10.9.

Table 3 Chirgwin-Coulson weights (in %) of the salicylic acid resonance structures resulting from the SC.1 and XCSC.1 calculations for all the considered basis-sets.

Structures	6-31G		6-311G		6-31G(d)		6-311G(d)	
	SC.1	XCSC.1	SC.1	XCSC.1	SC.1	XCSC.1	SC.1	XCSC.1
A	15.1	14.8	15.8	17.7	14.8	17.8	15.2	20.0
B	9.3	7.8	9.4	7.7	9.9	8.6	9.7	8.4
C	9.5	15.2	9.3	13.0	9.4	11.1	9.1	10.3
D	55.6	50.3	55.5	50.4	54.5	50.4	54.7	50.4
E	10.5	11.9	10.1	11.1	11.4	12.0	11.3	10.9

Also in this case we have completed the analysis of the SC.1 and XCSC.1 computations by analyzing the obtained spin-coupled orbitals and, in particular, by focusing on the orbitals variations when the X-ray data are directly taken into account in the calculations (see Figure 4). In most of the cases the trends are analogous to those observed in Figure 3 for the SC.0 and XCSC.0 calculations, even if with different intensities for the concentrations and depletions of electronic charge. Furthermore, as for the calculations based on unconstrained RHF molecular orbitals, it is possible to notice high similarities between the orbital variations resulting from the computations with the 6-31G and 6-311G basis-sets and, at the same time, between the orbitals variations obtained from the calculations exploiting basis-sets that include polarization functions.

However, the most important and evident difference between the XCSC.1-SC.1 and XCSC.0-SC.0 orbitals variations can be observed in the region of the carboxylic group, especially for orbitals φ_1, φ_5 and φ_6. We have previously pointed out that, using basis-sets 6-31G(d) and 6-311G(d), the XCSC.0 calculations provided orbitals φ_1, φ_5 and φ_6 characterized by significant charge redistributions on the carbon atom of the carboxylic group compared to the unconstrained computation (see Figure 3). Conversely, in Figure 4, we can observe that these charge redistributions disappear or significantly reduce when we consider the XCSC.1-SC.1 variations of the same orbitals. For orbital φ_1, if we consider the results of the computations with basis-sets 6-31G and 6-311G, we can even notice a slight depletion of electronic charge close the carboxylic group, which is not detected when the XCSC.0-SC.0 orbitals variations are considered. All these differences in the region of the carboxylic group actually derive from the different treatment of the inactive electrons in the X-ray constrained Spin-Coupled calculations. In fact, in our computations, only the 6 π electrons of the aromatic ring were fully treated at Spin-Coupled level, while the remaining ones (including those associated with the carboxylic group) were described by frozen doubly occupied molecular orbitals. In the XCSC.0 calculations, the molecular orbitals describing the electrons of the carboxylic group are obtained from unconstrained RHF computations and do not take into account the influence of the experimental X-ray diffraction data, which anyway contain information on the full electron density of the system (therefore, also on the electron density "basins" corresponding to the carboxylic group). Hence, the active spin-coupled orbitals (and the corresponding electron density distributions, see next subsection) resulting from the XCSC.0 calculations delocalize towards the carboxylic group to compensate the fact that the information contained in the X-ray diffraction data for the carboxylic group is not already captured by the frozen molecular orbitals used to describe the inactive electrons. On the contrary, when XCSC.1 calculations are carried out, the inactive electrons are described by orbitals resulting from XC-RHF computations and, therefore, the information contained in the X-ray data for the inactive electrons is already taken into account. This is probably the reason why in the active XCSC.1 orbitals (and in the related electron densities) the degree of the delocalization towards the carboxylic group is significantly lower.

The previous observation clearly reveals that, unlike the original version of the XCSC method (Genoni, Franchini *et al.*, 2018), the new X-ray constrained Spin-Coupled technique based on XC-RHF molecular orbitals enables to correctly deconvolute the X-ray constrained treatment of the inactive electrons from the one of the active electrons, thus leading to more balanced descriptions of the electronic structures and to better electron density distributions for the systems under exam.

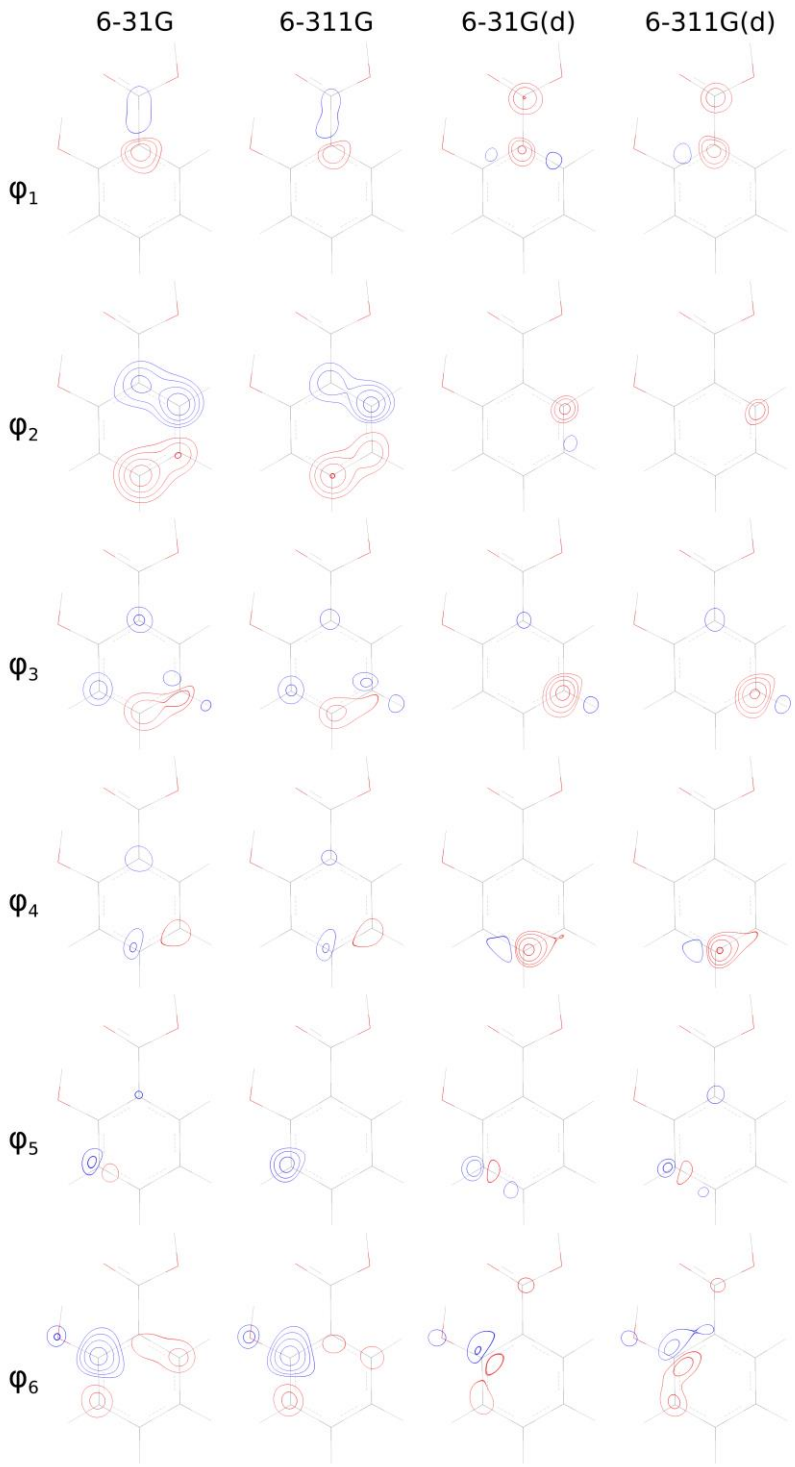

Figure 4 Two-dimensional plots of the differences between the square moduli of the XCSC.1 and SC.1 Spin-Coupled orbitals for all the considered basis-sets. The contours are drawn at $\pm 1 \cdot 10^{-3}$ e/bohr^3 and at $\pm 2, 4, 8 \cdot 10^{n}$ e/bohr^3 (with n as an integer ranging from -3 to 0) in a plane parallel to and 0.5 Å above the aromatic ring. Red and blue contours indicate positive and negative values, respectively.

3.4. Analysis of the obtained electron densities

Since X-ray structure factors used as constraints in XCW methods are strictly related to electron density, in our investigation we also analyzed the charge density distributions resulting from the performed calculations. In particular, we determined how the inclusion of the experimental structure factors in the XCSC computations influences the electron distributions. Therefore, we have evaluated and plotted the difference-maps between corresponding XCSC and SC electron densities, both for calculations using unconstrained RHF molecular orbitals and for calculations using XC-RHF molecular orbitals. These maps are depicted in Figure 5, where it can be easily noticed that the obtained differences are strictly related to the orbitals variations shown in Figures 2 and 3. For this reason, as for the orbitals variations, also in this case we observe high similarities between the difference-maps associated with basis-sets without polarization functions and between those corresponding to basis-sets including *d* functions. This is true both for the $\rho_{XCSC.0} - \rho_{SC.0}$ maps (see Figure 5, left panel) and for the $\rho_{XCSC.1} - \rho_{SC.1}$ maps (see Figure 5, right panel).

Analyzing Figure 5 in more detail, the difference-maps obtained with basis-sets 6-31G and 6-311G are generally characterized by a charge density accumulation on atoms C1 and C5 (see Figure 1 for the labels of the atoms belonging to the aromatic ring) and in the C3-C4 bonding region. At the same time, they also present charge depletions on atoms C2, C3, C4 and C6. All these charge accumulations and depletions decrease in intensity when XC-RHF molecular orbitals are used in the SC and XCSC computations. Furthermore, we can observe that, while in the $\rho_{XCSC.0} - \rho_{SC.0}$ maps there is a slight accumulation of charge on the carbon atom belonging to the carboxylic group, in the $\rho_{XCSC.1} - \rho_{SC.1}$ maps it is actually possible to observe a slight charge depletion for the same atom. An analogous trend can be observed for atom C5 when basis-set 6-311G is used. These trends and the observation that the intensities of charge accumulations and depletions decrease in the $\rho_{XCSC.1} - \rho_{SC.1}$ maps can be ascribed again to the fact that, in the SC.1 and XCSC.1 calculations, XC-RHF orbitals are used to describe the inactive electrons. As explained in the previous subsection, these orbitals already take into account the effects of the experimental data and enable to deconvolute the treatment of the active electrons from the one of the inactive electrons, thus leading to better descriptions of the electronic structures and to better electron densities.

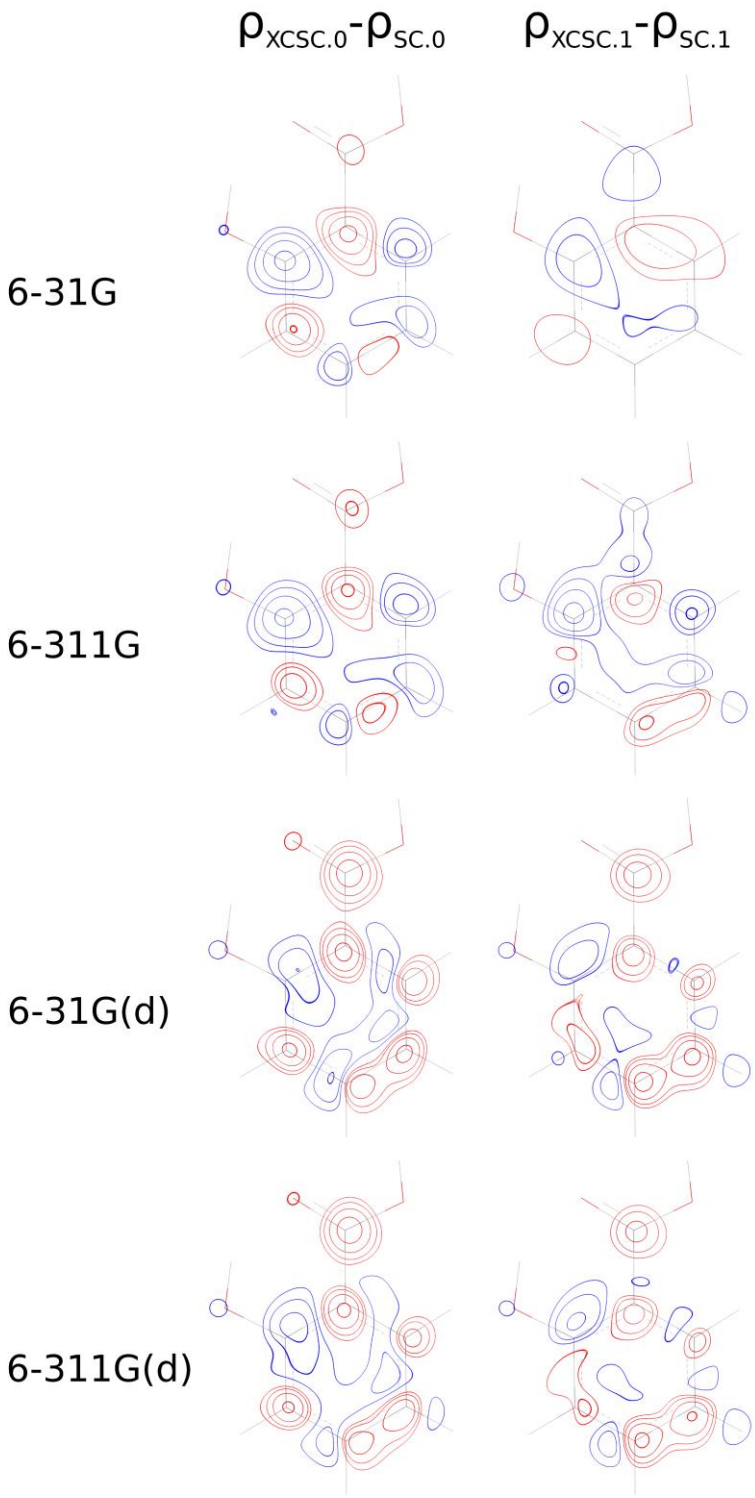

Figure 5 Two-dimensional plots of the differences between X-ray constrained and unconstrained Spin-Coupled electron densities for all the considered basis-sets. The contours are drawn at $\pm 1 \cdot 10^{-3}$ e/bohr^3 and at $\pm 2, 4, 8 \cdot 10^{n}$ e/bohr^3 (with n as an integer ranging from -3 to 0) in a plane parallel to and 0.5 Å above the aromatic ring. Red and blue contours indicate positive and negative values, respectively.

However, unlike the difference-densities obtained for basis-sets without polarization functions, those corresponding to basis sets 6-31G(d) and 6-311G(d) are more similar, regardless of the use of XC-RHF orbitals in the computations. In particular, charge accumulations are mainly observed for almost all the atoms belonging to the aromatic ring and for the carbon atom of the carboxylic group, while charge depletions are seen in the bonding regions and for atom C6. However, also in this case, in the $\rho_{XCSC.1} - \rho_{SC.1}$ maps we have noted a slight decrease of the intensities (especially for the carboxylic group region), which is again due to the use of X-ray constrained orbitals to treat the inactive electrons.

Finally, to perform a more global comparison, we have also computed similarity indexes between the obtained electron densities. In particular, we have adopted the Walker-Mezey similarity measure $L(\rho_x, \rho_y, a, a')$ (Walker & Mezey, 1994), which allows the comparison of two charge distributions ρ_x and ρ_y in a three-dimensional region bound by two isosurfaces characterized by the values a and a' (hereinafter indicated in e/bohr^3; see Supporting Information for more details about this similarity index). By changing a and a', the similarities between the electron densities can be evaluated in different 3D basins. Therefore, for all our comparisons, two Walker-Mezey similarity indexes have been taken into account: *i)* the $L(\rho_x, \rho_y, 0.1, 10)$ index to compare the electron densities in regions close to the nuclei (core regions); *ii)* $L(\rho_x, \rho_y, 0.001, 0.1)$ index to compare the charge distributions in the valence regions.

At first, we focused on the similarities between all the XCSC.1 electron densities. Both in the core and valence regions (see Tables 4 and 5, respectively), the Walker-Mezey similarity index confirms what was already observed in Figure 5, namely the fact that charge distributions obtained with the same kind of basis-set (i.e., with or without polarization functions) are generally more similar between each other. Completely analogous results have been obtained for the XCSC.0 electron distributions (see Tables S1 and S2 in the Supporting Information).

Table 4 Values of the Walker-Mezey similarity index $L(\rho_x, \rho_y, 0.1, 10)$ corresponding to the comparisons of the XCSC.1 electron densities obtained with the different basis-sets.

$L(\rho_x, \rho_y, 0.1, 10)$	6-31G	6-311G	6-31G(d)	6-311G(d)
6-31G	100.00			
6-311G	99.24	100.00		
6-31G(d)	97.31	97.52	100.00	
6-311G(d)	97.44	97.71	99.47	100.00

Table 5 Values of the Walker-Mezey similarity index $L(\rho_x, \rho_y, 0.001, 0.1)$ corresponding to the comparisons of the XCSC.1 electron densities obtained with the different basis-sets.

$L(\rho_x, \rho_y, 0.001, 0.1)$	6-31G	6-311G	6-31G(d)	6-311G(d)
6-31G	100.00			
6-311G	95.38	100.00		
6-31G(d)	93.36	92.09	100.00	
6-311G(d)	92.47	93.57	95.89	100.00

Afterwards, we compared the complete set of electron densities obtained for each basis-set. For the sake of clarity, we here report and discuss only the results obtained for basis set 6-31G(d) (see Tables 6 and 7), but completely analogous results have been obtained also for the other sets of basis functions (see Tables S3-S8 in the Supporting Information). In Table 6, which shows the values for similarity index $L(\rho_x, \rho_y, 0.1, 10)$, we can see that all the electron distributions resulting from calculations based on unconstrained RHF molecular orbitals (RHF, SC.0 and XCSC.0) are very similar (values greater than 99%). This holds true also for the electron densities associated with computations based on XC-RHF molecular orbitals (XC-RHF, SC.1 and XCSC.1). This observation is obviously in line with the fact that, for the two different families of computations, the real core electrons (which are a subset of the inactive electrons) have been treated in exactly the same way.

Finally, in Table 7, we show the values for index $L(\rho_x, \rho_y, 0.001, 0.1)$, which measures the degree of similarity in the valence region. Also in this case, despite lower values for the similarity indexes, it is easy to distinguish the two different groups of electron densities (in one group: RHF, SC.0 and XCSC.0; in the other one: XC-RHF, SC.1 and XCSC.1). It is interesting to notice that, for the first group, the similarity with the RHF electron density clearly decreases from SC.0 to XCSC.0. This is a clear indication of the different way in which we determined the orbitals that describe the active electrons for the system under exam (i.e., the 6 π electrons of the aromatic ring). In fact, in the RHF and SC.0 calculations, these orbitals have been obtained by simply minimizing the energy of the molecule, while, in the XCSC.0 case, they resulted from the minimization of the Jayatilaka functional. Conversely, in the second group of electron distributions, the similarity with the XC-RHF charge slightly increases passing from SC.1 to XCSC.1. This is due to the fact that, in the XC-RHF and XCSC.1 wave functions, the active electrons are described by orbitals that include the effect of the experimental X-ray diffraction data, while, in the SC.1 computations, the Spin-Coupled orbitals for the active electrons are obtained by only minimizing the energy functional, without introducing the constraint of the experimental structure factors. The effect of this different treatment also obviously

reflects in the lower value of the similarity index between the SC.1 and XCSC.1 electron density distributions.

Table 6 Values of the Walker-Mezey similarity index $L(\rho_x, \rho_y, 0.1, 10)$ corresponding to the comparisons of all the electron densities obtained with basis-set 6-31G(d).

$L(\rho_x, \rho_y, 0.1, 10)$	RHF	SC.0	XCSC.0	XC-RHF	SC.1	XCSC.1
RHF	100.00					
SC.0	99.61	100.00				
XCSC.0	99.15	99.34	100.00			
XC-RHF	97.04	97.25	97.56	100.00		
SC.1	97.16	97.39	97.57	99.65	100.00	
XCSC.1	96.88	97.09	97.45	99.75	99.47	100.00

Table 7 Values of the Walker-Mezey similarity index $L(\rho_x, \rho_y, 0.001, 0.1)$ corresponding to the comparisons of all the electron densities obtained with basis-set 6-31G(d).

$L(\rho_x, \rho_y, 0.001, 0.1)$	RHF	SC.0	XCSC.0	XC-RHF	SC.1	XCSC.1
RHF	100.00					
SC.0	98.59	100.00				
XCSC.0	96.52	97.57	100.00			
XC-RHF	93.50	94.23	93.84	100.00		
SC.1	94.19	94.81	93.24	98.63	100.00	
XCSC.1	92.79	93.53	93.91	98.77	97.63	100.00

4. Conclusions and perspectives

In this paper, we have presented the novel X-ray constrained Spin-Coupled method, a technique that introduces the typical high chemical interpretability of the Spin-Coupled strategy of Quantum Chemistry into the X-ray constrained wave function approach of Quantum Crystallography. In particular, we have shown the detailed derivation of the fundamental equations for the new method and we have discussed the results of further test calculations that were performed to better evaluate the capabilities of the proposed strategy.

The tests have revealed that the XCSC computations are quite straightforward and that the new strategy does not present particular convergence problems compared to the corresponding unconstrained Spin-Coupled technique. In analogy with results obtained by means of other X-ray constrained wave function methods, our calculations have also shown that the novel strategy provides better results and better statistical agreements with the experimental X-ray diffraction data as larger and more flexible basis-sets are used. Furthermore, as we initially expected, the new XCSC technique has always provided better (i.e., lower) χ^2 values compared to all the other strategies taken into account for the comparison.

One of the advantages of the novel XCSC consists in extracting the weights of the resonance structures for the system under investigation that are compatible with the X-ray structure factors observed experimentally. Notwithstanding some unavoidable variations in the absolute values, the X-ray constrained Spin-Coupled calculations generally provided resonance weights that changed consistently and with very similar trends when the X-ray diffraction data have been considered, practically regardless of the used basis-set.

Furthermore, to evaluate the effects of including the experimental structure factors in the calculations, we have also compared the obtained spin-coupled orbitals and electron densities, particularly focusing on the direct comparison between corresponding unconstrained and X-ray constrained quantities. The results indicate that the XCSC procedure entails clear redistributions of the electron density, which are generally similar for all the performed calculations. However, they sometimes show also some discrepancies depending on the adopted basis-set and, above all, on the treatment of the inactive electrons in the computations. In fact, compared to the original version of the X-ray constrained Spin-Coupled method (Genoni, Franchini *et al.*, 2018), in this paper we have introduced a further advancement of the technique consisting in using molecular orbitals obtained from a preliminary XC-RHF calculation to describe the inactive electrons in the XCSC procedure. The analysis of the obtained orbitals and electron densities have highlighted that the use of this new strategy enables to better deconvolute the description of the inactive electrons from the one of the active electrons, which consequently gives better and more balanced descriptions of the electronic structures for the systems under exam. Therefore, this will definitely be the procedure to follow for future XCSC computations and, for this reason, the new X-ray constrained Spin-Coupled technique can be also fully classified as the first post-XC-RHF method.

Finally, in the present study, we have proposed a new possible criterion to stop the XCW procedure, which consists in halting the computations when a clear inflection point is detected in the graph representing the trend of the χ^2 statistical agreement in function of the external multiplier λ. So far, the new criterion has been tested only for XCSC calculations and, at least for them, it seems robust and consistent. Anyway, further computational tests will be obviously necessary also on other types of X-ray constrained wave function methods to test its general applicability.

In conclusion, in this paper we have introduced a new X-ray constrained wave function strategy able to improve the description provided by the traditional X-ray constrained Hartree-Fock approach. Moreover, one of the main advantages of the novel strategy is that traditional chemical information (i.e., resonance structure weights, but also spatial distributions of the electronic clouds around atoms) can be directly obtained without imposing any preliminary constraint *a priori* or applying techniques *a posteriori* to the obtained wave function. However, notwithstanding the promising results obtained with the new method, here we do not claim the superiority of our novel approach over the existing ones. On the contrary, we want to point out that the proposed XCSC strategy will be only one of the different tools currently available in Quantum Crystallography to investigate chemical/physical problems/phenomena in the solid-state from different perspectives. In fact, each technique has its own features and provides specific answers. Therefore, as already highlighted by Fugel *et al.* (Fugel, Beckmann *et al.*, 2018), we believe that only the application of different and complementary methods can lead to a more global and complete description of the physical reality.

Concerning the future perspectives of the method, two aspects should be considered. First of all, it is worth pointing out that the proposed XCSC technique is a real many-determinant X-ray constrained wave function strategy. For this reason, it might be fruitfully used to obtain two-particle density matrices from experimental scattering data and also to shed further light on the capability of the XCW approach to capture electron correlation effects, a problem that, so far, has been investigated only inspecting how the wave function fitting reflects on the electron density (Genoni *et al.*, 2017; Grabowsky, 2017), but without taking into account quantities more strictly related to electron correlation (e.g., two-particle quantities as the intracule densities). In the context of these investigations, we are also planning to evaluate the capabilities of the XCSC method when the external constraints are only the low-angle reflections, which are those reflections that actually contain information on the electron correlation effects (Genoni *et al.*, 2017). Finally, considering that spin-coupled wave functions are exact spin-eigenfunctions also in case of open-shell systems, another tantalizing future perspective for the XCSC approach is its extension to the joint refinement of X-ray diffraction and Polarized Neutron diffraction data, with the final goal of obtaining experimental spin densities, which could be analysed through advanced quantum chemical topology techniques (Gatti *et al.*, 2015; Gatti *et al.*, 2017; Macetti *et al.*, 2018). This will be in line with techniques already developed in this context, as those proposed in the framework of the multipole models (Deutsch *et al.*, 2012; Deutsch *et al.*, 2014; Voufack *et al.*, 2017) and those already based on a wave function *ansatz* (Guedidda *et al.*, 2018).

Appendix A. Further theoretical details

A1. Higher order supercofactors

As we will show in section A2, supercofactors play a fundamental role in the XCSC method for the computation of the first and second derivatives of the Jayatilaka functional and can be actually defined in a very general way for the generic order *r*:

$$\mathfrak{D}(t_1\ t_2\ \dots\ t_r|\ u_1\ u_2\ \dots\ u_r) = \\ = \sum_{i,j=1}^{N_d} b_{S,i}\ b_{S,j}\ I^{ij}_{t_1u_1}\ I^{ij}_{t_2u_2}\ \dots\ I^{ij}_{t_ru_r}\ \mathcal{E}_{t_1t_2\dots t_r}\ \mathcal{E}_{u_1u_2\dots u_r}\ (-1)^{\sum_{k=1}^{r} t_k+u_k}\ \det\left[\boldsymbol{O_{ij}}(t_1t_2\dots t_r|u_1u_2\dots u_r)\right] \quad (25)$$

where symbols $\left\{I^{ij}_{t_ku_k}\right\}$ are analogous to the one in equation (22), $\boldsymbol{O_{ij}}(t_1t_2\dots t_r|u_1u_2\dots u_r)$ is the (*N*-*r*)-th order matrix obtained by deleting rows $t_1, t_2, \dots, t_r$ and columns $u_1, u_2, \dots, u_r$ of matrix $\boldsymbol{O_{ij}}$ and $\mathcal{E}_{v_1v_2\dots v_r}$ is a kind of Levi-Civita symbol related to the number of permutations that lead from the collection of integer numbers $(v_1v_2\dots v_r)$ to the ordered collection $(v'_1v'_2\dots v'_r)$ with $v'_1 < v'_2 < \dots < v'_r$. In particular, the symbol is defined like this:

$$\mathcal{E}_{v_1v_2\dots v_r} = \begin{cases} +1 & \text{for an even number of permutations} \\ -1 & \text{for an odd number of permutations} \end{cases} \quad (26)$$

By applying the Laplace theorem for the computation of the determinants, it is possible to show that every supercofactor of order *r* can be expressed in terms of the supercofactors of order *r+1* through the following recurrence relation:

$$\mathfrak{D}(t_1\ t_2\ \dots\ t_r|\ u_1\ u_2\ \dots\ u_r) = \sum_{w\neq t_1,t_2,\dots,t_r}^{N} \langle\phi_w\ |\ \phi_v\rangle\ \mathfrak{D}(t_1\ t_2\ \dots\ t_r\ w\ |\ u_1\ u_2\ \dots\ u_r\ v) \quad (27)$$

where ϕ_v and ϕ_w can be "core" or Spin-Coupled orbitals in wave function (19), while *v* is a dummy index that can be arbitrary chosen provided that it is different from the indices appearing in the "ket part" of the *r*-th order supercofactor. For the development of the traditional and the new X-ray constrained Spin-Coupled methods, it is also important to introduce two other classes of supercofactors: *i)* the indexed supercofactors and *ii)* the symmetrized indexed supercofactors. For the generic order *r*, the former are defined like this:

$$\mathfrak{D}_k(t_1\ t_2\ \dots\ t_r|\ u_1\ u_2\ \dots\ u_r) = \\ = \sum_{i,j=1}^{N_d} b_{S,i}\ d_{j,k}\ I^{ij}_{t_1u_1}\ I^{ij}_{t_2u_2}\ \dots\ I^{ij}_{t_ru_r}\ \mathcal{E}_{t_1t_2\dots t_r}\ \mathcal{E}_{u_1u_2\dots u_r}\ (-1)^{\sum_{k=1}^{r} t_k+u_k}\ \det\left[\boldsymbol{O_{ij}}(t_1t_2\dots t_r|u_1u_2\dots u_r)\right] \quad (28)$$

where $d_{j,k}$ represents the weight of the *j*-th Slater determinant in the *k*-th Spin-Coupled structure. Consequently, always for the generic *r*-th order, the latter are

$$\mathfrak{D}''_k(t_1\ t_2\ \dots\ t_r|\ u_1\ u_2\ \dots\ u_r) = \mathfrak{D}_k(t_1\ t_2\ \dots\ t_r|\ u_1\ u_2\ \dots\ u_r) + \mathfrak{D}_k(u_1\ u_2\ \dots\ u_r|\ t_1\ t_2\ \dots\ t_r) \quad (29)$$

It is easy to show that this relation exists between ordinary supercofactors and indexed supercofactors:

$$\mathfrak{D}(t_1\ t_2\ \dots\ t_r|\ u_1\ u_2\ \dots\ u_r) = \sum_{k=1}^{f_S^{N_v}} c_{S,k}\ \mathfrak{D}_k(t_1\ t_2\ \dots\ t_r|\ u_1\ u_2\ \dots\ u_r) \quad (30)$$

Furthermore, the following two other properties are also valid and exploited in the derivation of the working equations for the XCSC technique:

$$\mathfrak{D}\big(\hat{Q}[t_1\ t_2\ \dots\ t_r]\ \big|\ \hat{Q}[\ u_1\ u_2\ \dots\ u_r]\big) = \mathfrak{D}(t_1\ t_2\ \dots\ t_r|\ u_1\ u_2\ \dots\ u_r) \quad (31),$$

where $\hat{Q}$ is a generic permutation of the symmetric group of order *r*, and

$$\mathfrak{D}(u_1\ u_2\ \dots\ u_r|\ t_1\ t_2\ \dots\ t_r) = \mathfrak{D}(t_1\ t_2\ \dots\ t_r|\ u_1\ u_2\ \dots\ u_r) \quad (32)$$

However, while equation (31) is valid for every class of supercofactors, relation (32) can be used only for the ordinary and the symmetrized indexed ones.

A2. Derivatives of the χ^2 statistical agreement

To obtain the derivatives of functional (23), we clearly need both the derivatives of its energy part W and the derivatives of the statistical agreement between experimental and theoretical structure factors amplitudes, with the latter that must be obviously multiplied by λ and added to the former. The energy derivatives are identical to those already exploited in the traditional Spin-Coupled method (Cooper *et al.*, 1993) and, therefore, in this subsection, we will only focus on the formal derivation of the first and second derivatives of χ^2 with respect to the coefficients of the Spin-Coupled orbitals and with respect to the spin-coupling coefficients.

Exploiting the fact that $\left|F_{\boldsymbol{h}}^{calc}\right| = \left[F_{\boldsymbol{h}}^{calc}\left(F_{\boldsymbol{h}}^{calc}\right)^*\right]^{1/2}$, the first derivative of χ^2 with respect to a generic variable x can be written like this:

$$\frac{\partial\chi^2}{\partial x} = \sum_{\boldsymbol{h}} \frac{K_{\boldsymbol{h}}}{2}\left(\frac{\partial F_{\boldsymbol{h}}^{calc}}{\partial x}\left(F_{\boldsymbol{h}}^{calc}\right)^* + F_{\boldsymbol{h}}^{calc}\frac{\partial\left(F_{\boldsymbol{h}}^{calc}\right)^*}{\partial x}\right) \quad (33)$$

where x can be a generic spin-coupled orbital coefficient $C_{\mu k}$ or a generic spin-coupling coefficient $c_{s,k}$ and where

$$K_{\boldsymbol{h}} = \frac{2\eta}{N_r - N_p}\frac{\eta\left|F_{\boldsymbol{h}}^{calc}\right| - \left|F_{\boldsymbol{h}}^{exp}\right|}{\sigma_{\boldsymbol{h}}^2\left|F_{\boldsymbol{h}}^{calc}\right|} \quad (34)$$

Furthermore, since we assume to work with real orbitals, both for the first derivatives with respect to $C_{\mu k}$ and for the first derivatives with respect to $c_{s,k}$, it is possible to show that

$$\frac{\partial\left(F_{\boldsymbol{h}}^{calc}\right)^{*}}{\partial x}=\left(\frac{\partial F_{\boldsymbol{h}}^{calc}}{\partial x}\right)^{*} \quad (35)$$

and, consequently, equation (33) can be simply rewritten like this:

$$\frac{\partial\chi^{2}}{\partial x}=\sum_{\boldsymbol{h}}K_{\boldsymbol{h}}\left[\mathrm{Re}\left\{F_{\boldsymbol{h}}^{calc}\right\}\mathrm{Re}\left\{\frac{\partial F_{\boldsymbol{h}}^{calc}}{\partial x}\right\}+\mathrm{Im}\left\{F_{\boldsymbol{h}}^{calc}\right\}\mathrm{Im}\left\{\frac{\partial F_{\boldsymbol{h}}^{calc}}{\partial x}\right\}\right] \quad (36)$$

Now, introducing the definition of structure factor operator

$$\hat{I}_{\boldsymbol{h}}=\sum_{j=1}^{N_m}e^{i2\pi\left(\boldsymbol{Q}_j\boldsymbol{r}+\boldsymbol{q}_j\right)\cdot\boldsymbol{Bh}}=\hat{I}_{\boldsymbol{h},R}+i\,\hat{I}_{\boldsymbol{h},C} \quad (37)$$

where $\hat{I}_{\boldsymbol{h},R}$ and $\hat{I}_{\boldsymbol{h},C}$ (real and imaginary parts of $\hat{I}_{\boldsymbol{h}}$, respectively) are Hermitian operators, and exploiting equations (1) and (21), we obtain:

$$F_{\boldsymbol{h}}^{calc}=F_{\boldsymbol{h}}^{core}+\frac{F_{\boldsymbol{h}}^{SC}}{\mathfrak{D}}=2\sum_{t=1}^{N_1}\left\langle\,\phi_t^c\,\middle|\,\hat{I}_{\boldsymbol{h}}\,\middle|\,\phi_t^c\,\right\rangle+\frac{1}{\mathfrak{D}}\sum_{t,u=1}^{N_v}\left\langle\,\varphi_t\middle|\,\hat{I}_{\boldsymbol{h}}\,\middle|\,\varphi_u\right\rangle\mathfrak{D}(t|u) \quad (38)$$

Therefore, considering that $F_{\boldsymbol{h}}^{core}$ depends neither on the Spin-Coupled orbitals nor on the spin-coupling coefficients, the first derivatives of the calculated structure factors can be expressed in this way

$$\frac{\partial F_{\boldsymbol{h}}^{calc}}{\partial x}=-\frac{F_{\boldsymbol{h}}^{SC}}{\mathfrak{D}^{2}}\frac{\partial\mathfrak{D}}{\partial x}+\frac{1}{\mathfrak{D}}\frac{\partial F_{\boldsymbol{h}}^{SC}}{\partial x} \quad (39)$$

and the expression for the first derivatives of the statistical agreement becomes:

$$\frac{\partial\chi^{2}}{\partial x}=\sum_{\boldsymbol{h}}K_{\boldsymbol{h}}\left[\mathrm{Re}\left\{F_{\boldsymbol{h}}^{calc}\right\}\left(-\frac{\mathrm{Re}\left\{F_{\boldsymbol{h}}^{SC}\right\}}{\mathfrak{D}^{2}}\frac{\partial\mathfrak{D}}{\partial x}+\frac{1}{\mathfrak{D}}\mathrm{Re}\left\{\frac{\partial F_{\boldsymbol{h}}^{SC}}{\partial x}\right\}\right)\right.$$
$$\left.+\,\mathrm{Im}\left\{F_{\boldsymbol{h}}^{calc}\right\}\left(-\frac{\mathrm{Im}\left\{F_{\boldsymbol{h}}^{SC}\right\}}{\mathfrak{D}^{2}}\frac{\partial\mathfrak{D}}{\partial x}+\frac{1}{\mathfrak{D}}\mathrm{Im}\left\{\frac{\partial F_{\boldsymbol{h}}^{SC}}{\partial x}\right\}\right)\right] \quad (40)$$

where we have exploited the fact that $\mathfrak{D}$ is a real quantity.

From equation (40) it clearly follows that, in order to compute the first derivatives of χ^2, other than the calculated structure factors given by equation (38), it is also necessary to know the first derivatives $\partial\mathfrak{D}/\partial x$ and $\partial F_{\boldsymbol{h}}^{SC}/\partial x$.

First of all, let us consider the first derivatives with respect to the coefficients of the Spin-Coupled orbitals and, for the sake of example, let us consider in detail the mathematical derivation of the analytical expression for $\partial F_{\boldsymbol{h}}^{SC}/\partial C_{\mu k}$. To this purpose, let us expand $F_{\boldsymbol{h}}^{SC}$ in this way:

$$F_{\boldsymbol{h}}^{SC} = \sum_{t\neq k}^{N_v}\sum_{u\neq k}^{N_v} \langle \varphi_t | \hat{I}_{\boldsymbol{h}} | \varphi_u \rangle \, \mathfrak{D}(t|u) + \sum_{u\neq k}^{N_v} \langle \varphi_k | \hat{I}_{\boldsymbol{h}} | \varphi_u \rangle \, \mathfrak{D}(k|u) + \sum_{t\neq k}^{N_v} \langle \varphi_t | \hat{I}_{\boldsymbol{h}} | \varphi_k \rangle \, \mathfrak{D}(t|k) + \langle \varphi_k | \hat{I}_{\boldsymbol{h}} | \varphi_k \rangle \, \mathfrak{D}(k|k) \quad (41)$$

By using the properties of supercofactors (particularly, equation (32)) and bearing in mind that we assume to work with real orbitals, we easily obtain:

$$\frac{\partial F_{\boldsymbol{h}}^{SC}}{\partial C_{\mu k}} = \sum_{t\neq k}^{N_v}\sum_{u\neq k}^{N_v} \langle \varphi_t | \hat{I}_{\boldsymbol{h}} | \varphi_u \rangle \frac{\partial \mathfrak{D}(t|u)}{\partial C_{\mu k}} + \sum_{u\neq k}^{N_v} \langle \varphi_k | \hat{I}_{\boldsymbol{h}} | \varphi_u \rangle \frac{\partial \mathfrak{D}(k|u)}{\partial C_{\mu k}} + \sum_{t\neq k}^{N_v} \langle \varphi_t | \hat{I}_{\boldsymbol{h}} | \varphi_k \rangle \frac{\partial \mathfrak{D}(t|k)}{\partial C_{\mu k}} + 2\sum_{u=1}^{N_v} \langle \chi_\mu | \hat{I}_{\boldsymbol{h}} | \varphi_u \rangle \, \mathfrak{D}(k|u) \quad (42)$$

Now, exploiting recurrence relation (27), $\mathfrak{D}(t|u)$ can be simply expressed like this:

$$\mathfrak{D}(t|u) = \sum_{r\neq u}^{N_v} \langle \varphi_k | \varphi_r \rangle \;\; \mathfrak{D}(tk|ur) \quad (43)$$

and $\partial\mathfrak{D}(t|u)/\partial C_{\mu k}$ becomes:

$$\frac{\partial \mathfrak{D}(t|u)}{\partial C_{\mu k}} = \langle \chi_\mu | \varphi_k \rangle \, \mathfrak{D}(tk|uk) + \langle \varphi_k | \chi_\mu \rangle \, \mathfrak{D}(tk|uk) + \sum_{r\neq u,k}^{N_v} \langle \chi_\mu | \varphi_r \rangle \, \mathfrak{D}(tk|ur) + \sum_{r\neq u,k}^{N_v} \langle \varphi_k | \varphi_r \rangle \frac{\partial \mathfrak{D}(tk|ur)}{\partial C_{\mu k}} \quad (44)$$

Using again recurrence relation (27) for $\mathfrak{D}(tk|ur)$, we have:

$$\mathfrak{D}(tk|ur) = \sum_{s\neq t,k}^{N_v} \langle \varphi_s | \varphi_k \rangle \;\; \mathfrak{D}(tks|urk) \quad (45)$$

and, therefore, equation (44) can be rewritten like this:

$$\frac{\partial \mathfrak{D}(t|u)}{\partial C_{\mu k}} = \langle \chi_\mu | \varphi_k \rangle \, \mathfrak{D}(tk|uk) + \langle \varphi_k | \chi_\mu \rangle \, \mathfrak{D}(tk|uk) + \sum_{r\neq u,k}^{N_v} \langle \chi_\mu | \varphi_r \rangle \, \mathfrak{D}(tk|ur) + \sum_{s\neq t,k}^{N_v} \langle \varphi_s | \chi_\mu \rangle \sum_{r\neq u,k}^{N_v} \langle \varphi_k | \varphi_r \rangle \, \mathfrak{D}(tks|urk) \quad (46)$$

Now, since $\mathfrak{D}(tks|urk)$ is equivalent to $\mathfrak{D}(tsk|ukr)$ (see equation (31)), by exploiting the recurrence relation for supercofactors in the reverse way, we obtain

$$\sum_{r\neq u,k}^{N_v} \langle\varphi_k|\varphi_r\rangle\, \mathfrak{D}(tsk|ukr) = \mathfrak{D}(ts|uk) \quad (47)$$

Therefore, introducing (47) into (46), we can write

$$\frac{\partial \mathfrak{D}(t|u)}{\partial C_{\mu k}} = \sum_{r\neq u}^{N_v} \langle\chi_\mu|\,\varphi_r\rangle\, \mathfrak{D}(tk|ur) + \sum_{s\neq t}^{N_v} \langle\chi_\mu|\varphi_s\rangle\; \mathfrak{D}(ts|uk) \quad (48)$$

Furthermore, always exploiting recurrence relation (27), the other derivatives of the first-order supercofactor appearing in (42) can be expressed like this:

$$\frac{\partial \mathfrak{D}(k|u)}{\partial C_{\mu k}} = \sum_{r\neq k}^{N_v} \langle\chi_\mu|\,\varphi_r\rangle\, \mathfrak{D}(kr|uk) \quad (49)$$

and

$$\frac{\partial \mathfrak{D}(t|k)}{\partial C_{\mu k}} = \sum_{r\neq u}^{N_v} \langle\chi_\mu|\,\varphi_r\rangle\, \mathfrak{D}(tk|kr) \quad (50)$$

Now, using relations (48), (49) and (50) into (42), we obtain

$$\begin{aligned}\frac{\partial F_{\boldsymbol{h}}^{SC}}{\partial C_{\mu k}} = &\sum_{t\neq k}^{N_v}\sum_{u=1}^{N_v}\sum_{r\neq u}^{N_v} \langle\,\varphi_t|\,\hat{I}_{\boldsymbol{h}}\,|\,\varphi_u\rangle\,\langle\chi_\mu|\,\varphi_r\rangle\,\mathfrak{D}(tk|ur)\\ &+\sum_{t=1}^{N_v}\sum_{u\neq k}^{N_v}\sum_{r\neq t}^{N_v} \langle\,\varphi_t|\,\hat{I}_{\boldsymbol{h}}\,|\,\varphi_u\rangle\,\langle\chi_\mu|\,\varphi_r\rangle\,\mathfrak{D}(tr|uk)\\ &+2\sum_{t=1}^{N_v} \langle\,\chi_\mu|\,\hat{I}_{\boldsymbol{h}}\,|\,\varphi_t\rangle\,\mathfrak{D}(k|t) \qquad (51)\end{aligned}$$

Finally, considering that $\mathfrak{D}(tr|uk)$ is equivalent to $\mathfrak{D}(uk|tr)$ (see relation (32)) and exchanging the labels *t* and *u* in the second term of the right-hand side of the previous equation, the expression of $\partial F_{\boldsymbol{h}}^{SC}/\partial C_{\mu k}$ can be simply written in this way:

$$\frac{\partial F_{\boldsymbol{h}}^{SC}}{\partial C_{\mu k}} = 2\left[\sum_{t\neq k}^{N_v}\sum_{u=1}^{N_v}\sum_{r\neq u}^{N_v} \langle\,\varphi_t|\,\hat{I}_{\boldsymbol{h}}\,|\,\varphi_u\rangle\,\langle\chi_\mu|\,\varphi_r\rangle\,\mathfrak{D}(tk|ur) + \sum_{t=1}^{N_v} \langle\,\chi_\mu|\,\hat{I}_{\boldsymbol{h}}\,|\,\varphi_t\rangle\,\mathfrak{D}(k|t)\right] \quad (52)$$

By means of a similar mathematical procedure, namely by expanding supercofactors in terms of the higher-order ones and by exploiting the supercofactors properties (in particular properties (31) and (32)), it is also possible to obtain the analytical expression for the first derivatives of $\mathfrak{D}$ with respect to the coefficients of the Spin-Coupled orbitals:

$$\frac{\partial \mathfrak{D}}{\partial C_{\mu k}} = 2\sum_{r=1}^{N_v} \langle \chi_\mu |\, \varphi_r \rangle\, \mathfrak{D}(k|r) \qquad (53)$$

Now, let us take into account the first derivatives with respect to the spin-coupling coefficients $\{c_{S,k}\}$. In this regard, it is worth observing that the derivative of any r-th order ordinary supercofactor gives a symmetrized indexed supercofactor of the same order:

$$\frac{\partial \mathfrak{D}(t_1\, t_2 \ldots\, t_r |\, u_1\, u_2 \ldots\, u_r)}{\partial c_{S,k}} = \mathfrak{D}''_k(t_1\, t_2 \ldots\, t_r |\, u_1\, u_2 \ldots\, u_r) \qquad (54)$$

Therefore, exploiting the previous property and using the analytical expressions of $F_{\boldsymbol{h}}^{SC}$ and $\mathfrak{D}$ in equations (38) and (18), respectively, it is easy to see that:

$$\frac{\partial F_{\boldsymbol{h}}^{SC}}{\partial c_{S,k}} = \sum_{t,u=1}^{N_v} \langle\, \varphi_t |\, \hat{I}_{\boldsymbol{h}}\, |\, \varphi_u \rangle\, \mathfrak{D}''_k(t|\, u) \qquad (55)$$

and

$$\frac{\partial \mathfrak{D}}{\partial c_{S,k}} = \mathfrak{D}''_k \qquad (56)$$

As mentioned above, to determine the coefficients of the Spin-Coupled orbitals and the spin-coupling coefficients that minimize functional (23), the second derivatives of χ^2 are also necessary. To obtain their analytical form, let us start from equation (33) and let us derive it with respect to the generic variable y. In compact form, we can write:

$$\frac{\partial^2 \chi^2}{\partial y\, \partial x} = \sum_{\boldsymbol{h}} K_{\boldsymbol{h}} \frac{\partial A_{\boldsymbol{h}}}{\partial y} + \frac{\partial K_{\boldsymbol{h}}}{\partial y}\, A_{\boldsymbol{h}} \qquad (57)$$

where $A_{\boldsymbol{h}}$ is given by

$$\begin{aligned} A_{\boldsymbol{h}} &= \frac{1}{2}\left(\frac{\partial F_{\boldsymbol{h}}^{calc}}{\partial x}\, \left(F_{\boldsymbol{h}}^{calc}\right)^* + F_{\boldsymbol{h}}^{calc} \frac{\partial \left(F_{\boldsymbol{h}}^{calc}\right)^*}{\partial x} \right) = \\ &= \mathrm{Re}\{F_{\boldsymbol{h}}^{calc}\} \left(-\frac{\mathrm{Re}\{F_{\boldsymbol{h}}^{SC}\}}{\mathfrak{D}^2} \frac{\partial \mathfrak{D}}{\partial x} + \frac{1}{\mathfrak{D}}\, \mathrm{Re}\left\{ \frac{\partial F_{\boldsymbol{h}}^{SC}}{\partial x} \right\} \right) \\ &+ \mathrm{Im}\{F_{\boldsymbol{h}}^{calc}\} \left(-\frac{\mathrm{Im}\{F_{\boldsymbol{h}}^{SC}\}}{\mathfrak{D}^2} \frac{\partial \mathfrak{D}}{\partial x} + \frac{1}{\mathfrak{D}}\, \mathrm{Im}\left\{ \frac{\partial F_{\boldsymbol{h}}^{SC}}{\partial x} \right\} \right) \end{aligned} \qquad (58)$$

and where $\partial K_{\boldsymbol{h}}/\partial y$ is

$$\frac{\partial K_{\boldsymbol{h}}}{\partial y} = \Gamma_{\boldsymbol{h}} \left[\frac{\mathrm{Re}\{F_{\boldsymbol{h}}^{calc}\}}{|F_{\boldsymbol{h}}^{calc}|^3} \left(-\frac{\mathrm{Re}\{F_{\boldsymbol{h}}^{SC}\}}{\mathfrak{D}^2} \frac{\partial \mathfrak{D}}{\partial y} + \frac{1}{\mathfrak{D}} \mathrm{Re}\left\{ \frac{\partial F_{\boldsymbol{h}}^{SC}}{\partial y} \right\} \right) + \frac{\mathrm{Im}\{F_{\boldsymbol{h}}^{calc}\}}{|F_{\boldsymbol{h}}^{calc}|^3} \left(-\frac{\mathrm{Im}\{F_{\boldsymbol{h}}^{SC}\}}{\mathfrak{D}^2} \frac{\partial \mathfrak{D}}{\partial y} + \frac{1}{\mathfrak{D}} \mathrm{Im}\left\{ \frac{\partial F_{\boldsymbol{h}}^{SC}}{\partial y} \right\} \right) \right] \quad (59)$$

with

$$\Gamma_{\boldsymbol{h}} = \frac{2\eta \, |F_{\boldsymbol{h}}^{exp}|}{(N_r - N_p)\, \sigma_{\boldsymbol{h}}^2} \quad (60)$$

Therefore, equation (58) and equation (59) depend only on $F_{\boldsymbol{h}}^{calc}$ and on the first derivatives of $F_{\boldsymbol{h}}^{SC}$ and $\mathfrak{D}$, which are already known. On the contrary, if we consider the derivative $\partial A_{\boldsymbol{h}}/\partial y$, we have:

$$\frac{\partial A_{\boldsymbol{h}}}{\partial y} = \frac{1}{2} \left(\frac{\partial^2 F_{\boldsymbol{h}}^{calc}}{\partial y \, \partial x} \left(F_{\boldsymbol{h}}^{calc}\right)^* + \frac{\partial F_{\boldsymbol{h}}^{calc}}{\partial x} \frac{\partial \left(F_{\boldsymbol{h}}^{calc}\right)^*}{\partial y} + \frac{\partial F_{\boldsymbol{h}}^{calc}}{\partial y} \frac{\partial \left(F_{\boldsymbol{h}}^{calc}\right)^*}{\partial x} + F_{\boldsymbol{h}}^{calc} \frac{\partial^2 \left(F_{\boldsymbol{h}}^{calc}\right)^*}{\partial y \partial x} \right) \quad (61)$$

Also in this case, since we assume to work with real orbitals, both for the second derivatives with respect to the coefficients of the Spin-Coupled orbitals and for the second derivatives with respect to the spin-coupling coefficients, it is possible to show that

$$\frac{\partial^2 \left(F_{\boldsymbol{h}}^{calc}\right)^*}{\partial y \partial x} = \left(\frac{\partial^2 F_{\boldsymbol{h}}^{calc}}{\partial y \, \partial x} \right)^* \quad (62)$$

Therefore, taking into account relations (35) and (62), we obtain:

$$\frac{\partial A_{\boldsymbol{h}}}{\partial y} = \mathrm{Re}\{F_{\boldsymbol{h}}^{calc}\} \mathrm{Re}\left\{ \frac{\partial^2 F_{\boldsymbol{h}}^{calc}}{\partial y \, \partial x} \right\} + \mathrm{Re}\left\{ \frac{\partial F_{\boldsymbol{h}}^{calc}}{\partial x} \right\} \mathrm{Re}\left\{ \frac{\partial F_{\boldsymbol{h}}^{calc}}{\partial y} \right\} + \mathrm{Im}\{F_{\boldsymbol{h}}^{calc}\} \mathrm{Im}\left\{ \frac{\partial^2 F_{\boldsymbol{h}}^{calc}}{\partial y \, \partial x} \right\} + \mathrm{Im}\left\{ \frac{\partial F_{\boldsymbol{h}}^{calc}}{\partial x} \right\} \mathrm{Im}\left\{ \frac{\partial F_{\boldsymbol{h}}^{calc}}{\partial y} \right\} \quad (63)$$

Now, starting from equation (39), we have

$$\frac{\partial^2 F_{\boldsymbol{h}}^{calc}}{\partial y \partial x} = 2 \frac{F_{\boldsymbol{h}}^{SC}}{\mathfrak{D}^3} \frac{\partial \mathfrak{D}}{\partial y} \frac{\partial \mathfrak{D}}{\partial x} - \frac{1}{\mathfrak{D}^2} \frac{\partial \mathfrak{D}}{\partial x} \frac{\partial F_{\boldsymbol{h}}^{SC}}{\partial y} - \frac{F_{\boldsymbol{h}}^{SC}}{\mathfrak{D}^2} \frac{\partial^2 \mathfrak{D}}{\partial y \partial x} - \frac{1}{\mathfrak{D}^2} \frac{\partial \mathfrak{D}}{\partial y} \frac{\partial F_{\boldsymbol{h}}^{SC}}{\partial x} + \frac{1}{\mathfrak{D}} \frac{\partial^2 F_{\boldsymbol{h}}^{SC}}{\partial y \partial x} \quad (64)$$

and substituting (39) and (64) into (63), $\partial A_{\boldsymbol{h}}/\partial y$ becomes:

$$\frac{\partial A_{\boldsymbol{h}}}{\partial y} = \mathrm{Re}\{F_{\boldsymbol{h}}^{calc}\}\left(\frac{2\,\mathrm{Re}\{F_{\boldsymbol{h}}^{SC}\}}{\mathfrak{D}^3}\frac{\partial \mathfrak{D}}{\partial y}\frac{\partial \mathfrak{D}}{\partial x} - \frac{1}{\mathfrak{D}^2}\frac{\partial \mathfrak{D}}{\partial x}\,\mathrm{Re}\left\{\frac{\partial F_{\boldsymbol{h}}^{SC}}{\partial y}\right\} - \frac{\mathrm{Re}\{F_{\boldsymbol{h}}^{SC}\}}{\mathfrak{D}^2}\frac{\partial^2 \mathfrak{D}}{\partial y \partial x} - \frac{1}{\mathfrak{D}^2}\frac{\partial \mathfrak{D}}{\partial y}\,\mathrm{Re}\left\{\frac{\partial F_{\boldsymbol{h}}^{SC}}{\partial x}\right\} + \frac{1}{\mathfrak{D}}\,\mathrm{Re}\left\{\frac{\partial^2 F_{\boldsymbol{h}}^{SC}}{\partial y \partial x}\right\}\right)$$
$$+\ \mathrm{Im}\{F_{\boldsymbol{h}}^{calc}\}\left(\frac{2\,\mathrm{Im}\{F_{\boldsymbol{h}}^{SC}\}}{\mathfrak{D}^3}\frac{\partial \mathfrak{D}}{\partial y}\frac{\partial \mathfrak{D}}{\partial x} - \frac{1}{\mathfrak{D}^2}\frac{\partial \mathfrak{D}}{\partial x}\,\mathrm{Im}\left\{\frac{\partial F_{\boldsymbol{h}}^{SC}}{\partial y}\right\} - \frac{\mathrm{Im}\{F_{\boldsymbol{h}}^{SC}\}}{\mathfrak{D}^2}\frac{\partial^2 \mathfrak{D}}{\partial y \partial x} - \frac{1}{\mathfrak{D}^2}\frac{\partial \mathfrak{D}}{\partial y}\,\mathrm{Im}\left\{\frac{\partial F_{\boldsymbol{h}}^{SC}}{\partial x}\right\} + \frac{1}{\mathfrak{D}}\,\mathrm{Im}\left\{\frac{\partial^2 F_{\boldsymbol{h}}^{SC}}{\partial y \partial x}\right\}\right)$$
$$+\left(-\frac{\mathrm{Re}\{F_{\boldsymbol{h}}^{SC}\}}{\mathfrak{D}^2}\frac{\partial \mathfrak{D}}{\partial x} + \frac{1}{\mathfrak{D}}\,\mathrm{Re}\left\{\frac{\partial F_{\boldsymbol{h}}^{SC}}{\partial x}\right\}\right)\left(-\frac{\mathrm{Re}\{F_{\boldsymbol{h}}^{SC}\}}{\mathfrak{D}^2}\frac{\partial \mathfrak{D}}{\partial y} + \frac{1}{\mathfrak{D}}\,\mathrm{Re}\left\{\frac{\partial F_{\boldsymbol{h}}^{SC}}{\partial y}\right\}\right)$$
$$+\left(-\frac{\mathrm{Im}\{F_{\boldsymbol{h}}^{SC}\}}{\mathfrak{D}^2}\frac{\partial \mathfrak{D}}{\partial x} + \frac{1}{\mathfrak{D}}\,\mathrm{Im}\left\{\frac{\partial F_{\boldsymbol{h}}^{SC}}{\partial x}\right\}\right)\left(-\frac{\mathrm{Im}\{F_{\boldsymbol{h}}^{SC}\}}{\mathfrak{D}^2}\frac{\partial \mathfrak{D}}{\partial y} + \frac{1}{\mathfrak{D}}\,\mathrm{Im}\left\{\frac{\partial F_{\boldsymbol{h}}^{SC}}{\partial y}\right\}\right) \quad (65)$$

Therefore, it is clear that $\partial A_{\boldsymbol{h}}/\partial y$ does not depend only on $F_{\boldsymbol{h}}^{calc}$ and on the first derivatives of $F_{\boldsymbol{h}}^{SC}$ and $\mathfrak{D}$, but also on the second derivatives $\partial^2 F_{\boldsymbol{h}}^{SC}/\partial y\,\partial x$ and $\partial^2 \mathfrak{D}/\partial y\,\partial x$, which will be discussed below.

Let us consider the orbital-orbital second derivatives of $F_{\boldsymbol{h}}^{SC}$ and $\mathfrak{D}$, namely the second derivatives of $F_{\boldsymbol{h}}^{SC}$ and $\mathfrak{D}$ only with respect to the coefficients of the Spin-Coupled orbitals. These second derivatives can be obtained by following the mathematical procedure already adopted to derive the expression of $\partial F_{\boldsymbol{h}}^{SC}/\partial C_{\mu k}$, namely by exploiting the properties of the supercofactors and, in particular, by using recurrence relation (27). Nevertheless, since these derivations require a large number of steps, here, for the sake of simplicity, we will report only the final analytical expressions of the second derivatives. It is necessary to distinguish between two different cases: *i)* the simplest one, in which the derivatives are with respect to two coefficients of the same Spin-Coupled orbital (case $h = k$) and *ii)* the one in which the derivatives are with respect to two coefficients of different Spin-Coupled orbitals (case $h \neq k$).

Let us consider the case $h = k$. It is possible to show that:

$$\frac{\partial^2 F_{\boldsymbol{h}}^{SC}}{\partial C_{\nu k}\partial C_{\mu k}} = 2\Bigg[\sum_{t\neq k}^{N_v}\sum_{u\neq k}^{N_v}\sum_{r\neq u,k}^{N_v}\sum_{s\neq t,k}^{N_v}\langle\,\varphi_t|\,\hat{I}_{\boldsymbol{h}}\,|\,\varphi_u\rangle\,\langle\chi_\mu|\,\varphi_r\rangle\,\langle\chi_\nu|\,\varphi_s\rangle\;\mathfrak{D}(tks|urk)$$
$$+\sum_{t\neq k}^{N_v}\sum_{u\neq k}^{N_v}\langle\,\varphi_t|\,\hat{I}_{\boldsymbol{h}}\,|\,\varphi_u\rangle\,\langle\chi_\mu|\chi_\nu\rangle\;\mathfrak{D}(tk|uk)$$
$$+\sum_{t\neq k}^{N_v}\sum_{r\neq k}^{N_v}\left(\langle\,\chi_\nu|\,\hat{I}_{\boldsymbol{h}}\,|\,\varphi_t\rangle\,\langle\chi_\mu|\,\varphi_r\rangle+\langle\,\chi_\mu|\,\hat{I}_{\boldsymbol{h}}\,|\,\varphi_t\rangle\,\langle\chi_\nu|\,\varphi_r\rangle\right)\mathfrak{D}(tk|kr)$$
$$+\langle\,\chi_\mu|\,\hat{I}_{\boldsymbol{h}}\,|\chi_\nu\rangle\;\mathfrak{D}(k|k)\Bigg] \qquad (66)$$

and

$$\frac{\partial^2 \mathfrak{D}}{\partial C_{\nu k}\partial C_{\mu k}} = 2\left[\sum_{r\neq k}^{N_v}\sum_{s\neq k}^{N_v}\langle\chi_\mu|\,\varphi_r\rangle\,\langle\chi_\nu|\,\varphi_s\rangle\,\mathfrak{D}(ks|rk)+\langle\chi_\mu|\chi_\nu\rangle\,\mathfrak{D}(k|k)\right] \qquad (67)$$

For the case $h \neq k$ the derivation is slightly more cumbersome and we obtain:

$$\frac{\partial^2 F_{\boldsymbol{h}}^{SC}}{\partial C_{\nu h}\partial C_{\mu k}} = 2\Bigg[\sum_{t\neq k,h}^{N_v}\sum_{u=1}^{N_v}\sum_{r\neq u}^{N_v}\sum_{s\neq u,r}^{N_v}\langle\,\varphi_t|\,\hat{I}_{\boldsymbol{h}}\,|\,\varphi_u\rangle\,\langle\chi_\mu|\,\varphi_r\rangle\,\langle\chi_\nu|\,\varphi_s\rangle\;\mathfrak{D}(tkh|urs)$$
$$+\sum_{t\neq k}^{N_v}\sum_{u\neq h}^{N_v}\sum_{r\neq u,h}^{N_v}\sum_{s\neq t,k}^{N_v}\langle\,\varphi_t|\,\hat{I}_{\boldsymbol{h}}\,|\,\varphi_u\rangle\,\langle\chi_\mu|\,\varphi_r\rangle\,\langle\chi_\nu|\,\varphi_s\rangle\;\mathfrak{D}(tks|urh)$$
$$+\sum_{t\neq k}^{N_v}\sum_{u\neq h}^{N_v}\langle\,\varphi_t|\,\hat{I}_{\boldsymbol{h}}\,|\,\varphi_u\rangle\,\langle\chi_\mu|\chi_\nu\rangle\;\mathfrak{D}(tk|uh)$$
$$+\sum_{t\neq k}^{N_v}\sum_{r\neq h}^{N_v}\langle\,\chi_\nu|\,\hat{I}_{\boldsymbol{h}}\,|\,\varphi_t\rangle\,\langle\chi_\mu|\,\varphi_r\rangle\;\mathfrak{D}(tk|hr)$$
$$+\sum_{u=1}^{N_v}\sum_{r\neq u}^{N_v}\langle\,\chi_\nu|\,\hat{I}_{\boldsymbol{h}}\,|\,\varphi_u\rangle\,\langle\chi_\mu|\,\varphi_r\rangle\;\mathfrak{D}(hk|ur)$$
$$+\sum_{t=1}^{N_v}\sum_{s\neq t}^{N_v}\langle\,\chi_\mu|\,\hat{I}_{\boldsymbol{h}}\,|\,\varphi_t\rangle\,\langle\chi_\nu|\,\varphi_s\rangle\;\mathfrak{D}(kh|ts)+$$
$$+\sum_{t\neq h}^{N_v}\sum_{s\neq k}^{N_v}\langle\,\chi_\mu|\,\hat{I}_{\boldsymbol{h}}\,|\,\varphi_t\rangle\,\langle\chi_\nu|\,\varphi_s\rangle\,\mathfrak{D}(ks|th)+\langle\,\chi_\mu|\,\hat{I}_{\boldsymbol{h}}\,|\chi_\nu\rangle\,\mathfrak{D}(k|h)\Bigg] \qquad (68)$$

and

$$\frac{\partial^2 \mathfrak{D}}{\partial C_{\nu h}\partial C_{\mu k}} = 2\left[\sum_{r=1}^{N_v}\sum_{s\neq r}^{N_v}\langle\chi_\mu|\,\varphi_r\rangle\,\langle\chi_\nu|\,\varphi_s\rangle\,\mathfrak{D}(kh|rs) + \sum_{r\neq h}^{N_v}\sum_{s\neq k}^{N_v}\langle\chi_\mu|\,\varphi_r\rangle\,\langle\chi_\nu|\,\varphi_s\rangle\;\mathfrak{D}(ks|rh) + \langle\chi_\mu|\chi_\nu\rangle\;\mathfrak{D}(k|h)\right] \quad (69)$$

Now, let us take into account the spin-orbital second derivatives of $F_{\boldsymbol{h}}^{SC}$ and $\mathfrak{D}$. Unlike the orbital-orbital second derivatives, the derivation is really straightforward. In fact, exploiting property (54) and applying it to equations (52) and (53), we easily obtain:

$$\frac{\partial^2 F_{\boldsymbol{h}}^{SC}}{\partial c_{S,h}\,\partial C_{\mu k}} = 2\left[\sum_{t\neq k}^{N_v}\sum_{u=1}^{N_v}\sum_{r\neq u}^{N_v}\langle\,\varphi_t|\,\hat{I}_{\boldsymbol{h}}\,|\,\varphi_u\rangle\,\langle\chi_\mu|\,\varphi_r\rangle\,\mathfrak{D}_h''(tk|ur) + \sum_{t=1}^{N_v}\langle\,\chi_\mu|\,\hat{I}_{\boldsymbol{h}}\,|\,\varphi_t\rangle\,\mathfrak{D}_h''(k|t)\right] \quad (70)$$

and

$$\frac{\partial^2 \mathfrak{D}}{\partial c_{S,h}\,\partial C_{\mu k}} = 2\sum_{r=1}^{N_v}\langle\chi_\mu|\,\varphi_r\rangle\;\mathfrak{D}_h''(k|r) \quad (71)$$

Finally, to obtain the analytical expressions of the spin-spin second derivatives of $F_{\boldsymbol{h}}^{SC}$ and $\mathfrak{D}$, namely the analytical expressions of the second derivatives only with respect to spin-coupling coefficients, we have used a different approach. To this purpose, let us start considering the spin-spin second derivatives of $\mathfrak{D}$. It is easy to see that, using equations (6) and (17), $\mathfrak{D}$ can be also expressed in this way:

$$\mathfrak{D} = \langle\,\Psi_0^{SC}|\,\Psi_0^{SC}\rangle = \sum_{p=1}^{f_S^{N_v}}\sum_{q=1}^{f_S^{N_v}} c_{S,p}\,c_{S,q}\,\langle\psi_{S,M;p}^{N}|\psi_{S,M;q}^{N}\rangle \quad (72)$$

Therefore, it is straightforward to show that:

$$\frac{\partial^2 \mathfrak{D}}{\partial c_{S,h}\,\partial c_{S,k}} = 2\,\langle\psi_{S,M;h}^{N}|\psi_{S,M;k}^{N}\rangle = 2\sum_{i,j=1}^{N_d} d_{i,h}\,d_{j,k}\,\langle\Omega_i|\Omega_j\rangle \quad (73)$$

where we have exploited the fact that each generic spin-coupled structure $\psi_{S,M;k}^{N}$ can be written as a linear combination of Slater determinants $\{\Omega_i\}$. The coefficients of the linear combination $\{d_{i,k}\}$ are identical to the coefficients in the expansion of the corresponding spin-eigenfunction in terms of spin primitive functions (see equation (12)).

In order to compute the spin-spin second derivatives of $F_{\boldsymbol{h}}^{SC}$, first of all it is worth nothing that, after introducing the N-electron structure factor operator

$$\hat{\mathfrak{I}}_{\boldsymbol{h}} = \sum_{a=1}^{N}\hat{I}_{\boldsymbol{h}}(\boldsymbol{x}_a) \quad (74),$$

$F_{\boldsymbol{h}}^{calc}$ can be rewritten like this:

$$F_{\boldsymbol{h}}^{calc} = \langle \Psi_0 | \widehat{\Im}_{\boldsymbol{h}} | \Psi_0 \rangle = F_{\boldsymbol{h}}^{core} + \frac{F_{\boldsymbol{h}}^{SC}}{\mathfrak{D}} =$$

$$= \frac{1}{\mathfrak{D}} \sum_{p=1}^{f_S^{N_v}} \sum_{q=1}^{f_S^{N_v}} c_{S,p}\, c_{S,q}\, \langle \psi_{S,M;p}^{N} | \widehat{\Im}_{\boldsymbol{h}} | \psi_{S,M;q}^{N} \rangle \qquad (75)$$

Therefore,

$$F_{\boldsymbol{h}}^{SC} = \sum_{p=1}^{f_S^{N_v}} \sum_{q=1}^{f_S^{N_v}} c_{S,p}\, c_{S,q}\, \langle \psi_{S,M;p}^{N} | \widehat{\Im}_{\boldsymbol{h}} | \psi_{S,M;q}^{N} \rangle - F_{\boldsymbol{h}}^{core}\, \mathfrak{D} \qquad (76)$$

and it is easy to obtain:

$$\frac{\partial^2 F_{\boldsymbol{h}}^{SC}}{\partial c_{S,h}\, \partial c_{S,k}} = 2\, \langle \psi_{S,M;h}^{N} | \widehat{\Im}_{\boldsymbol{h}} | \psi_{S,M;k}^{N} \rangle - F_{\boldsymbol{h}}^{core} \frac{\partial^2 \mathfrak{D}}{\partial c_{S,h}\, \partial c_{S,k}} =$$

$$= 2 \sum_{i,j=1}^{N_d} d_{i,h}\, d_{j,k}\, \langle\, \Omega_i \,|\widehat{\Im}_{\boldsymbol{h}}|\, \Omega_j \rangle - F_{\boldsymbol{h}}^{core} \frac{\partial^2 \mathfrak{D}}{\partial c_{S,h}\, \partial c_{S,k}} \qquad (77)$$

with $\partial^2 \mathfrak{D} / \partial c_{S,h}\, \partial c_{S,k}$ given by equation (73).

References

Aleksandrov, Y. V., Tsirelson, V. G., Reznik. I. M. & Ozerov, R. P. (1989). *Phys. Status Solidi B* **155**, 201-207.

Bader, R. F. W. (1990). *Atoms in Molecules: A Quantum Theory*. Oxford (U.K.): Oxford University Press.

Becke, A. D. & Edgecombe, K. E. (1990) *J. Chem. Phys.* **92**, 5397-5403.

Bučinský, L., Jayatilaka, D. & Grabowsky, S. (2016). *J. Phys. Chem. A* **120**, 6650-6669.

Boys, S. F. (1960). *Rev. Mod. Phys.* **32**, 296–299.

Bytheway, I., Grimwood, D. J., Figgis, B. N., Chandler, G. S. & Jayatiaka, D. (2002). *Acta Cryst.* A**58,** 244−251.

Bytheway, I., Grimwood, D. J. & Jayatilaka, D. (2002). *Acta Cryst.* A**58**, 232−243.

Casati, N., Genoni, A., Meyer, B., Krawczuk, A. & Macchi, P. (2017). *Acta Cryst.* B**73**, 584-597.

Chirgwin, B. H. & Coulson, C. A. (1950). *Proc. R. Soc. London A* **201**, 196-209.

Clinton, W. L., Frishberg, C. A., Massa, L. J. & Oldfield, P. L. (1973). *Int. J. Quantum Chem.: Quantum Chem. Symp.* **7**, 505-514.

Clinton, W. L. & Massa, L. J. (1972). *Phys. Rev. Lett.* **29**, 1363-1366.

Cooper, D. L., Gerrat, J. & Raimondi, M. (1986). *Nature* **323**, 699-701.

Cooper, D. L., Gerrat, J. & Raimondi, M. (1991). *Chem. Rev.* **91**, 929-964.

Cooper, D. L., Gerratt, J., Raimondi, M., Sironi, M. & Thorsteinsson, T. (1993). *Theor. Chim. Acta* **85**, 261-270.

Deutsch, M., Claiser, N., Pillet, S., Chumakov, Y., Becker, P., Gillet, J.-M., Gillon, B., Lecomte, C. & Souhassou, M. (2012). *Acta Cryst.* A**68**, 675–686.

Deutsch, M., Gillon, B., Claiser, N., Gillet, J.-M., Lecomte, C. & Souhassou, M. (2014). *IUCrJ* **1**, 194–199.

Dewar, M. J. S. (1952). *J. Am. Chem. Soc.* **74**, 3341–3345.

Dos Santos, L. H. R., Genoni, A. & Macchi, P. (2014). *Acta Cryst.* A***70***, 532-551.

Edmiston, C. & Ruedenberg, K. (1963). *Rev. Mod. Phys.* **35**, 457–465.

Edmiston, C. & Ruedenberg, K. (1965) *J. Chem. Phys.* **43**, S97–S116.

Frisch, M. J., Trucks, G. W., Schlegel, H. B., Scuseria, G. E., Robb, M. A., Cheeseman, J. R., Scalmani, G., Barone, V., Mennucci, B., Petersson, G. A., Nakatsuji, H., Caricato, M., Li, X., Hratchian, H. P., Izmaylov, A. F., Bloino, J., Zheng, G., Sonnenberg, J. L., Hada, M., Ehara, M., Toyota, K., Fukuda, R., Hasegawa, J., Ishida, M., Nakajima, T., Honda, Y., Kitao, O., Nakai, H., Vreven, T., Montgomery, J. A. Jr., Peralta, J. E., Ogliaro, F., Bearpark, M., Heyd, J. J., Brothers, E., Kudin, K. N., Staroverov, V. N., Kobayashi, R., Normand, J., Raghavachari, K., Rendell, A., Burant, J. C., Iyengar, S. S., Tomasi, J., Cossi, M., Rega, N., Millam, J. M., Klene, M., Knox, J. E., Cross, J. B., Bakken, V., Adamo, C., Jaramillo, J., Gomperts, R., Stratmann, R. E., Yazyev, O., Austin, A. J., Cammi, R., Pomelli, C., Ochterski, J. W., Martin, R. L., Morokuma, K., Zakrzewski, V. G., Voth, G. A., Salvador, P., Dannenberg, J. J., Dapprich, S., Daniels, A. D., Farkas, Ö., Foresman, J. B., Ortiz, J. V., Cioslowski, J., Fox, D. J. (2009). *Gaussian 09, Revision D.01*. Wallingford (CT, USA): Gaussian, Inc.

Frishberg, C. & Massa, L. J. (1981). *Phys. Rev. B* **24**, 7018-7024.

Fornili, A., Sironi, M. & Raimondi, M. (2003). *J. Mol. Struct. (THEOCHEM)* **632**, 157–172.

Foster, J. M. & Boys, S. F. (1960). *Rev. Mod. Phys.* **32**, 300–302.

Fugel, M., Beckmann, J., Jayatilaka, D., Gibbs, G. V. & Grabowsky, S. (2018). *Chem. Eur. J.* **24**, 6248-6261.

Fugel, M., Kleemiss, F., Malaspina, L. A., Pal, R., Spackman, P. R., Jayatilaka, D. & Grabowsky, S. (2018). *Aust. J. Chem.* **71**, 227-237.

Gatti, C., Orlando, A. M. & Lo Presti, L. (2015) *Chem. Sci.* **6**, 3845-3852.

Gatti, C., Macetti, G. & Lo Presti, L. (2017) *Acta Cryst.* B**73**, 565-583.

Genoni, A. (2013a). *J. Phys. Chem. Lett.* **4**, 1093-1099.

Genoni, A. (2013b). *J. Chem. Theory Comput.* **9**, 3004-3019.

Genoni, A. (2017). *Acta Cryst.* A**73**, 312-316.

Genoni, A., Bučinský, L., Claiser, N., Contreras-García, J., Dittrich, B.; Dominiak, P. M., Espinosa, E., Gatti, C., Giannozzi, P., Gillet, J.-M., Jayatilaka, D., Macchi, P., Madse, A. Ø., Massa, L. J., Matta, C. F., Merz, K. M. Jr., Nakashima, P. N. H., Ott, H., Ryde, U., Schwarz, K., Sierka, M. & Grabowsky, S. (2018). *Chem. Eur. J.* **24**, 10881-10905.

Genoni, A., Dos Santos, L. H. R., Meyer, B. & Macchi, P. (2017). *IUCrJ* **4**, 136-146.

Genoni, A., Fornili, A. & Sironi, M. (2005). *J. Comput. Chem.* **26**, 827-835.

Genoni, A., Franchini, D., Pieraccini, S. & Sironi, M. (2018). *Chem. Eur. J.* **24**, 15507-15511.

Genoni, A., Ghitti, M., Pieraccini, S. & Sironi, M. (2005). *Chem. Phys. Lett.* **415**, 256-260.

Genoni, A. & Meyer, B. (2016). *Adv. Quantum Chem.* **73**, 333-362.

Genoni, A & Sironi, M. (2004). *Theor. Chem. Acc.* **112**, 254-262.

Gerratt, J. (1971). *Adv. Atom Mol. Phys.* **7**, 141-221.

Gerratt, J. & Lipscomb, W. N. (1968). *Proc. Natl. Acad. Sci. USA* **59**, 332-335.

Gilbert, T. L. (1975). *Phys. Rev. B* **12**, 2111-2120.

Gillet, J.-M. (2007). *Acta Cryst.* A**63**, 234-238.

Gillet, J.-M. & Becker, P. J. (2004). *J. Phys. Chem. Sol.* **65**, 2017-2023.

Gillet, J.-M., Becker, P. J. & Cortona, P. (2001). *Phys. Rev. B* **63**, 235115.

Glendening, E. D. & Weinhold, F. (1998). *J. Comput. Chem.* **19**, 593-609.

Goddard, W. A. III (1967). *Phys. Rev*. **157**, 81-93.

Goddard, W. A. III, Dunning, T. H. Jr., Hunt, W. J. & Hay, P. J. (1973). *Acc. Chem. Res.* **3**, 368-276.

Goldberg, M. J. & Massa, L. J. (1983). *Int. J. Quantum Chem.* **24**, 113-126.

Goldfield, S., Quandt, R. & Trotter, F. (1966). *Econometrica* **34**, 541-551.

Massa, L., Goldberg, M., Frishberg, C., Boehme, R. F. & La Placa, S. J. (1985). *Phys. Rev. Lett.* **55**, 622-625.

Grabowsky, S. (2017). *Acta Cryst.* A**73**, C568-C568.

Grabowsky, S., Genoni, A. & Bürgi, H.-B. (2017). *Chem. Sci.* **8**, 4159-4176.

Grabowsky, S., Jayatilaka, D., Mebs, S. & Luger, P. (2010). *Chem. Eur. J.* **16**, 12818-12821.

Grabowsky, S., Luger, P., Buschmann, J., Schneider, T., Schirmeister, T., Sobolev, A. N. & Jayatilaka, D. (2012). *Angew. Chem., Int. Ed.* **51**, 6776-6779.

Grabowsky, S., Weber, M., Jayatilaka, D., Chen, Y.-S., Grabowski, M. T., Brehme, R., Hesse, M., Schirmeister, T. & Luger, P. (2011). *J. Phys. Chem. A* **115**, 12715-12732.

Grimwood, D. J., Bytheway, I. & Jayatilaka, D. (2003). *J. Comput. Chem.* **24**, 470−483.

Grimwood, D. J. & Jayatilaka, D. (2001). *Acta Cryst.* A**57**, 87−100.

Guedidda, S., Yan, Z., Kibalin, I., Voufack, A. B., Claiser, N., Souhassou, M., Lecomte, C., Gillon, B. & Gillet, J.-M. (2018). *J. Chem. Phys.* **148**, 164106.

Hansen, N. K. & Coppens, P. (1978). *Acta Cryst.* A**34**, 909−921.

Heitler, W. & London, F. (1927). *Z. Phys.* **44**, 455-472.

Henderson, G. A. & Zimmermann, R. K. (1976). *J. Chem. Phys*. **65**, 619-622.

Hibbs, D. E., Howard, S. T., Huke, J. P. & Waller, M. P. (2005). *Phys. Chem. Chem. Phys.* **7**, 1772-1778.

Hiberty, P. C., Humbel. S., van Lenthe, J. H. & Byrman, C. P. (1994). *J. Chem. Phys.* **101**, 5969-5976.

Hiberty, P. C. & Shaik, S. (2007). *J. Comput. Chem.* **28**, 137-151.

Hirao, K., Nakano, H., Nakayama, K. & Dupuis, M. (1996). *J. Chem. Phys*. **105**, 9227-9239.

Hollauer, E. & Nascimento, M. A. C. (1993). *J. Chem. Phys*. **99**, 1207-1214.

Howard, S. T., Huke, J. P., Mallinson, P. R. & Frampton, C. S. (1994). *Phys. Rev. B* **49**, 7124-7136.

Hückel, E. (1930). Z. *Phys.* **60**, 423-456.

Hückel, E. (1931). Z. *Phys.* **72**, 310-337.

Hudák, M., Jayatilaka, D., Peraínova, L., Biskupic, S., Kozísek, J. & Bučinský, L. (2010). *Acta Cryst.* A**66**, 78−92.

Jayatilaka, D. (1998). *Phys. Rev. Lett.* **80**, 798-801.

Jayatilaka, D. (2012). *Modern Charge-Density Analysis* edited by C. Gatti & P. Macchi, pp. 213-257. Dordrecht: Springer Netherlands.

Jayatilaka, D., Grimwood, D. J. (2001). *Acta Cryst.* A**57**, 76−86.

Jayatilaka, D., Grimwood, D. J. (2003). *Computational Science – ICCS 2003*. Edited by P. M. A. Sloot, D. Abramson, A. V. Bogdanov, J. J. Dongarra, A. Y. Zomaya & Y. E. Gorbachev, pp. 142-151. Berlin & Heidelberg: Springer-Verlag.

Jayatilaka, D. & Grimwood, D. (2004) *Acta Cryst.* A**60**, 111-119.

Karadakov, P. B., Gerratt, J., Cooper, D. L. & Raimondi, M. (1992). *J. Chem. Phys.* **97**, 7637-7655.

Kohout, M. (2004). *Int. J. Quantum Chem.* **97**, 651-658.

Ladner, R. C. & Goddard, W. A. III (1969). *J. Chem. Phys.* **51**, 1073-1087.

London, F. (1928). *Z. Phys.* **46**, 455-477.

Löwdin, P.-O. (1955). *Phys. Rev.* **97**, 1474-1489.

Macetti, G., Lo Presti, L. & Gatti, C. (2018) *J. Comput. Chem.* **39**, 587-603.

Massa, L. & Matta, C. F. (2017). *J. Comput. Chem.* **39**, 1021-1028.

McDouall, J. J. W. (1992). *Theor. Chim. Acta* **83**, 339-350.

McWeeny, R. (1992). *Methods of Molecular Quantum Mechanics. Second Edition*. London (U.K.): Academic Press.

Meyer, B. & Genoni, A. (2018). *J. Phys. Chem. A* **122**, 8965-8981.

Meyer, B., Guillot, B., Ruiz-Lopez, M. F. & Genoni, A. (2016a). *J. Chem. Theory. Comput.* **12**, 1052-1067.

Meyer, B., Guillot, B., Ruiz-Lopez, M. F., Jelsch, C. & Genoni, A. (2016b). *J. Chem. Theory. Comput.* **12**, 1068-1081.

Munshi, P. & Guru-Row, T. N. (2006). *Acta Cryst.* B**62**, 612-626.

Novara, R. F., Genoni, A. & Grabowsky, S. (2018). *ChemViews*, DOI:10.1002/chemv.201800066.

Pauling, L. (1939). *The Nature of Chemical Bond. An Introduction to Modern Structural Chemistry*. Cornell University Press, Ithaca, NY, USA.

Pipek, J. & Mezey, P. G. (1989). *J. Chem. Phys.* **90**, 4916–4926.

Raimondi, M., Sironi, M., Gerrat, J. & Cooper, D. L. (1996). *Int. J. Quantum Chem.* **60**, 225-233.

Roothaan, C. C. J. (1951). *Rev. Mod. Phys.* **23**, 69-89.

Roversi, P., Irwin, J. J. & Bricogne, G. (1998). *Acta Cryst.* A**54**, 971–996.

Sakata, M. & Sato, M. (1990). *Acta Cryst.* A**46**, 263–270.

Song, L., Wu, W., Hiberty, P. C., Danovich, D. & Shaik, S. (2003). *Chem. Eur. J.* **9**, 4540-4547.

Schmider, H. L. & Becke, A. D. (2000). **527**, 51-61.

Schmider, H., Smith, V. H. Jr. & Weyrich, W. (1990). *Trans. Am. Crystallogr. Assoc.* **26**, 125-140.

Schmider, H., Smith, V. H. Jr. & Weyrich, W. (1992). *J. Chem. Phys.* **96**, 8986-8994.

Shurki, A. (2006). *Theor. Chem. Acc.* **116**, 253-261.

Simonetta, M., Gianinetti, E. & Vandoni, I. (1968). *J. Chem. Phys.* **48**, 1579-1594.

Sironi, M., Genoni, A., Civera, M., Pieraccini, S. & Ghitti, M. (2007). *Theor. Chem. Acc.* **117**, 685-698.

Sironi, M., Ghitti, M., Genoni, A., Saladino, G. & Pieraccini, S. (2009). *J. Mol. Struct. (THEOCHEM)* **898**, 8-16.

Snyder, J. A. & Stevens, E. D. (1999). *Chem. Phys. Lett.* **313**, 293-398.

Stewart, R. F. (1969). *J. Chem. Phys.* **51**, 4569-4577.

Stewart, R. F. (1976). *Acta Cryst.*. A**32**, 565−574.

Stoll, H., Wagenblast, G. & Preuss, H. (1980). *Theor. Chim. Acta* **57**, 169−178.

Tanaka, K. (1988). *Acta Cryst.* A**44**, 1002-1008.

Tanaka, K. (2018). *Acta Cryst.* A***74***, 345-356.

Thorsteinsson, T., Cooper, D. L., Gerrat, J., Karadakov, P. B. & Raimondi, M. (1996). *Theor. Chim. Acta* **93**, 343-366.

Tsirelson, V. (2017). *J. Comput. Chem.* **39**, 1029-1037.

Van Lenthe, J. H. & Balint-Kurti, G. G. (1983). *J. Chem. Phys.* **78**, 5699-5713.

Van Smaalen, S. & Netzel, J. (2009). *Phys. Scr.* **79**, 048304.

Voter, A. F. & Goddard, W. A. III. (1981). *J. Chem. Phys*. **75**, 3638-3639.

Voufack, A. B., Claiser, N., Lecomte, C., Pillet, S., Pontillon, Y., Gillon, B., Yan, Z., Gillet, J.-M., Marazzi, M., Genoni, A. & Souhassou, M. (2017). *Acta Cryst.* B**73**, 544-549.

Walker, P. D. & Mezey, P. G. (1994). *J. Am. Chem. Soc.* **116**, 12022-12032.

Waller, M. P., Howard, S. T., Platts, J. A., Piltz, R. O., Willock, D. J. & Hibbs, D. E. (2006). *Chem. Eur. J.* **12**, 7603-7614.

Weinhold, F. & Landis, C. R. (2001). *Chem. Educ. Res. Pract.* **2**, 91-104.

Weyrich, W. (2006). *Lect. Ser. Comput. Comput. Sci.* **5**,1-3.